

AD-A032 591

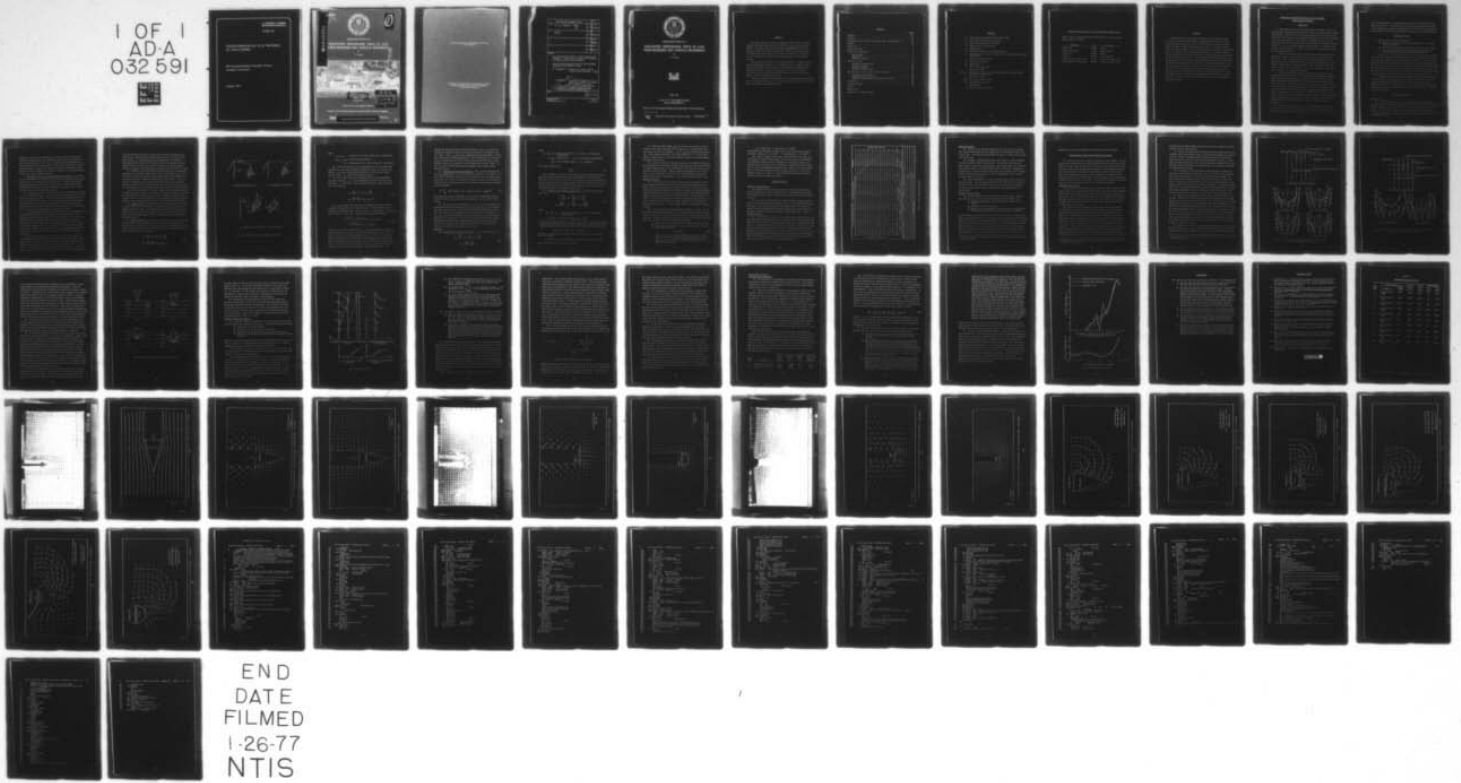
ARMY ENGINEER WATERWAYS EXPERIMENT STATION VICKSBURG MISS F/G 8/13
EVALUATING PENETRATION TESTS IN CLAY FROM MEASURED SOIL PARTICL--ETC(U)
FEB 71 Y T CHOU

UNCLASSIFIED

WES-MP-71-2

NL

1 OF 1
AD-A
032 591



U.S. DEPARTMENT OF COMMERCE
National Technical Information Service

AD-A032 591

EVALUATING PENETRATION TESTS IN CLAY FROM MEASURED
SOIL PARTICLE MOVEMENTS

ARMY ENGINEER WATERWAYS EXPERIMENT STATION,
VICKSBURG, MISSISSIPPI

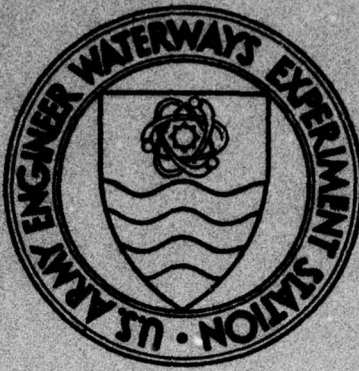
FEBRUARY 1971

T47

337067

71-2
3

0



AD A032591

MISCELLANEOUS PAPER M-71-2

EVALUATING PENETRATION TESTS IN CLAY FROM MEASURED SOIL PARTICLE MOVEMENTS

by

Y. T. Chou

US-CE-C

Property of the



REPRODUCED BY
NATIONAL TECHNICAL
INFORMATION SERVICE
U. S. DEPARTMENT OF COMMERCE
SPRINGFIELD, VA. 22161

February 1971

DDC
RECEIVED
NOV 27 1976
D

Sponsored by U. S. Army Materiel Command

Conducted by U. S. Army Engineer Waterways Experiment Station, Vicksburg, Mississippi

This document
may be moved

Approved for Public Release; Distribution Unlimited

foreign nationals

64

**Destroy this report when no longer needed. Do not return
it to the originator.**

**The findings in this report are not to be construed as an official
Department of the Army position unless so designated
by other authorized documents.**

ROUTING AND TRANSMITTAL SLIP		ACTION	
1 TO MR. W.G. SHOCKLEY (MESL) <i>WJH</i>	INITIALS	CIRCULATE	
	DATE	COORDINATION	
2 LIBRARY	INITIALS	FILE	
	DATE	INFORMATION	
3	INITIALS	NOTE AND RETURN	
	DATE	PER CON-VERSATION	
4	INITIALS	SEE ME	
	DATE	SIGNATURE	
REMARKS			
<p>DDC HAS REQUESTED MP-M-71-2 (COPY OF TITLE PAGE ATTACHED). WE ARE GOING TO SEND COPY ON LOAN AS NO RETENTION COPIES ARE AVAILABLE.</p> <p>COULD YOU PLEASE TELL US WHICH OF THE FOLLOWING DISTRIBUTION STATEMENTS TO USE?</p> <p><input checked="" type="checkbox"/> STATEMENT A Approved for public release; distribution unlimited. <i>WJH</i></p> <p><u>OR</u></p> <p>STATEMENT B: Distribution limited to U.S. Government agencies only; test and evaluation <u>date ?</u>.</p> <p>Other requests for this document must be referred to U.S. Army Materiel Command.</p> <p>Do NOT use this form as a RECORD of approvals, concurrences, disapprovals, clearances, and similar actions</p>			
FROM		DATE	
LIBRARY BRANCH, TIC		OCT 29 1976	
		PHONE	



MISCELLANEOUS PAPER M-71-2

EVALUATING PENETRATION TESTS IN CLAY FROM MEASURED SOIL PARTICLE MOVEMENTS

by

Y. T. Chou



February 1971

Sponsored by U. S. Army Materiel Command
Project IT061102B52A-01

Conducted by U. S. Army Engineer Waterways Experiment Station, Vicksburg, Mississippi

ARMY-MRC VICKSBURG, MISS.

This docu
may be r

Approved for Public Release; Distribution Unlimited

~~or foreign nationals~~

Foreword

The study reported herein was conducted in 1969 at the U. S. Army Engineer Waterways Experiment Station (WES) as a part of the vehicle mobility research program under DA Project 1T061102B52A, "Research in Military Aspects of Terrestrial Sciences," Task 01, "Military Aspects of Off-Road Mobility," under the sponsorship and guidance of the Research, Development and Engineering Directorate, U. S. Army Materiel Command.

The study was conceived and carried out by Dr. Y. T. Chou under the general supervision of Messrs. W. G. Shockley and S. J. Knight, Chief and Assistant Chief, respectively, of the Mobility and Environmental Division, and under the direct supervision of Dr. K. W. Wiendieck, former member of the Research Projects Group of the Mobility Research Branch. Dr. Chou prepared this report.

COL Levi A. Brown, CE, and COL Ernest D. Peixotto, CE, were Directors of the WES during the course of this study and preparation of this report. Mr. F. R. Brown was Technical Director.

Contents

	<u>Page</u>
Foreword	iii
Notation	vii
Conversion Factors, Metric to British Units of Measurement	ix
Summary	xi
Background	1
Purpose and Scope	2
Theoretical Background	2
Basic concept	2
Equations	7
Material constants	9
Laboratory Tests	10
Soil and its preparation	10
Sample preparation	10
Testing procedure	12
Accuracy of test method	12
Presentation of Test Results and Their Analysis	13
Laboratory test results	13
Computer program and results	19
Theoretical prediction of penetration resistance	24
Conclusions	28
Literature Cited	29
Table 1	
Plates 1-16	
Appendix A: Computer Program	

Notation

c_t	Soil cohesion determined from triaxial tests
CI	Cone index (penetration resistance)
J_2	Second invariant of stress tensor
K	Yield stress in simple shear
P	Vertical load
R	Resistance of soil to a probe (constant)
u,w	Displacements of soil in r (radial) and z (vertical) directions, respectively.
v	Velocity of soil movement
V	Penetration velocity
α, θ	Angles (fig. 1)
γ	Shear-strain component
Δ	Interval of time
$\epsilon_r, \epsilon_\theta, \epsilon_z$	Strains in r (radial), (circumferential), and z (vertical) directions, respectively
σ	Normal soil stress
σ'_{ij}	Deviatoric stress tensor
σ_θ	Circumferential stress
τ	Shear stress
ϕ	Angle of internal friction

Conversion Factors, Metric to British Units of Measurement

Metric units of measurement used in this report can be converted to British units as follows:

<u>Multiply</u>	<u>By</u>	<u>To Obtain</u>
centimeters	0.3937	inches
square centimeters	0.155	square inches
millimeters	0.0394	inches
newtons	0.2248	pounds (force)
kilonewtons per square meter	0.145	pounds per square inch
kilonewtons per cubic meter	6.3659	pounds per cubic inch

Summary

The deformation and flow characteristics of a near-saturated fat clay under penetration were studied. Penetrations were made in a 50.8-cm-diam mold with a circular cone, a circular plate, and two rectangular plates at speeds ranging from 0.004 to 5.6 cm/sec. The strain, strain rate, and velocity fields in the soil were calculated from the soil particle movements, determined by measuring the displacement of pellets embedded in the soil before penetration. Actual soil flow patterns determined from velocity fields were studied. It was found that if the deformation energy of the soil were assumed equal to the penetration energy, the former could be obtained by integration over the affected volume of the deformed soil. The penetration resistance was thus computed on the basis of the Von Mises yield criterion and compared with the measured penetration resistance. Computed and measured penetration resistance values were markedly different; this casts some doubt on the applicability of the Von Mises equation to results of tests on clay under penetration and on the computational procedure employed.

EVALUATING PENETRATION TESTS IN CLAY FROM MEASURED
SOIL PARTICLE MOVEMENTS

Background

1. Cone penetrometer tests have been used extensively at the U. S. Army Engineer Waterways Experiment Station (WES) to evaluate soil strength, and empirical correlations have been established between laboratory cone penetration resistance and tire performance parameters. The main advantage of the cone penetrometer is its inherent simplicity; but it must be recognized that basic soil properties, such as cohesion, internal friction, viscosity, etc., are not determined by this instrument. Therefore, the present trend in penetration studies heavily favors experimentation that yields empirical results.

2. Evaluation of cone penetration resistance of soil by relations based on the theory of continuum mechanics has not been particularly successful. Most of these analyses have been oriented toward static bearing capacity of footings and have not taken into consideration such factors as viscosity and inertia effects. Thus, while these theories assist somewhat in understanding the nature of a penetration test, they do not provide a means for evaluating it.

3. Recently, Yong¹⁰ and Miller⁶ developed a new approach toward rigid wheel-soil interaction. Using the concept of continuum mechanics, they approached the problem by an analytical-empirical method, viscoplasticity, which had previously been used successfully in analyzing metal processing. This method assumes that soil stresses under a wheel can be calculated if the velocity field within the soil is known. Yong and Miller determined the velocity field by sophisticated X-ray techniques. Strains and strain rates were computed, and the stress distribution was determined by a constitutive equation (the Von Mises plasticity equation) linking stresses and strain rates. Although this so-called viscoplasticity method has yielded no conclusive results, it seems promising.

4. In the study reported herein, the viscoplasticity method is applied to cone penetration tests. This problem is relatively simple compared to that of soil-wheel interaction. However, in contrast to the

work of Yong and Miller, the three-dimensionality of the problem is taken fully into account. It was hoped that the results would shed some light on the fundamental mechanics of penetration tests and allow the evaluation of the potential of the viscoplasticity method for more complex problems.

Purpose and Scope

5. The purposes of this study were to:

- a. Study the deformation and flow characteristics of the soil under penetration.
- b. Examine the Von Mises equation in light of the test results.
- c. Evaluate the potential of the viscoplasticity method for predicting soil-vehicle interaction theoretically.

6. Ten tests with four different probes--a circular cone, a circular plate, and two rectangular plates--were conducted in a 50.8-cm-diam* mold of heavy clay at speeds varying from 0.004 to 5.6 cm/sec. Only one soil was used; its moisture content averaged 50 percent, saturation ranged from 97 to 99 percent, and penetration resistance ranged from 38.8 to 129.5 kN/m². The strain, strain rate, and velocity fields in the soil were computed from the movements of soil particles. The movements were determined by measuring the displacement of pellets embedded in the soil before penetration.

7. Because of a lack of funds, the study was shortened and simplified considerably with respect to the original plan. Results from a circular cone and circular plate penetrating the soil at a very slow speed (0.004 cm/sec) were the only data used to compare measured and predicted penetration resistance, and results of the other tests are presented without further analysis.

Theoretical Background

Basic concept

8. In the basic concept of soil penetration problems in clay presented in this section, the validity of the theory of perfectly plastic solids and the selection of a relatively high-moisture-content clay for the test program are discussed. Also, the meaning of the velocity field and the

*A table of factors for converting metric to British units of measurement is given on page ix.

differences in the stress conditions in cases of plane strain and axisymmetry are pointed out, with particular emphasis on the significance of the circumferential stress σ_{θ} . An equation is formulated based on the principle of energy conservation. This equation equates the rate of input penetration energy to the rate of output soil deformation energy, and can be used to evaluate the physical constants of the material numerically or to check available theories.

9. Validity of the theory of perfectly plastic solids. According to the Mohr-Coulomb law, shear stress increases with normal stress on the failure plane for all but purely cohesive soils. Drucker and Prager³ generalized the Mohr-Coulomb law to account for all principal stresses, and Drucker² demonstrated that by applying the normality rule, a volume increase must accompany any plastic strain.

10. Upon application of a shear stress, soils undergo volume changes in a very complicated manner. Dense soils and overconsolidated clays increase in volume upon shear stress, but normally consolidated clays and loose sands decrease in volume. Also, sands can undergo further plastic strain without volume change once they have been strained far enough. Whitman⁹ pointed out that the observed rates of expansion of dense sands are far less than those predicted from plasticity theory.

11. In discussing the importance and necessity of the normality rule, Whitman⁹ quoted from a paper by Drucker, Gibson, and Henkel:⁴ "The normality rule is much more than simply an assumption. It is the inevitable consequence of making two less stringent and very reasonable assumptions: (a) isotropy and (b) a stable material. Also, the important upper and lower bound theories are valid only so long as the normality rule applies. Without the normality rule, we lose all theoretical justification for using such results as the Prandtl-Hill bearing capacity equations."

12. The general tendency in research on plastic flow problems of frictional materials is to retain the normality rule, but seek for other yield criteria. Strain rates do not remain normal to the Mohr-Coulomb yield surface, but are normal to another curved surface. The normality rule is satisfied if the curved surface is the yield surface. Drucker, Gibson, and Henkel⁴ proposed that the yield surface for soils should look

like the Mohr-Coulomb surface, except that it should be capped at the open end by a dome that would expand and contract as the volume of the soil changed. In research conducted at Massachusetts Institute of Technology (MIT) for the WES,¹ the yield surface was assumed to be elliptical and to be able to move along the stress axis during plastic strain, the plastic volume changing in proportion to the change in stress.

13. Although the concept developed at MIT seemed to be reasonable and promising, conclusive results have not yet been established. It is felt that a correct plasticity theory solving plastic flow problems for frictional materials cannot be obtained in the near future. Since the theory of perfectly plastic materials has been found to be sound when applied to nonfrictional materials, this study was limited to soft clay at a consistency near full saturation, which satisfied the condition $\phi = 0$.

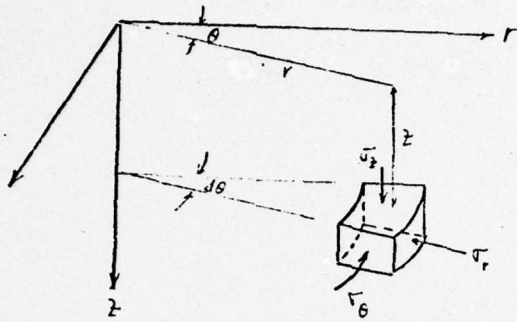
14. The clay tested had a moisture content of 50 percent, which was only about 3 percent short of saturation. The angle of internal friction ϕ determined from triaxial tests was zero. Although the high moisture content of the soil created difficulty and inconvenience in preparing the sample, it was overwhelmingly advantageous in the theoretical analysis.

15. Velocity field. Velocity fields in a soil mass show the directions and velocities of soil particle movements, or rather the flow or rupture patterns of soil. In this study, the velocity fields were computed from the measured soil particle movements, and the soil flow patterns under different shapes of probes penetrating at different speeds were investigated.

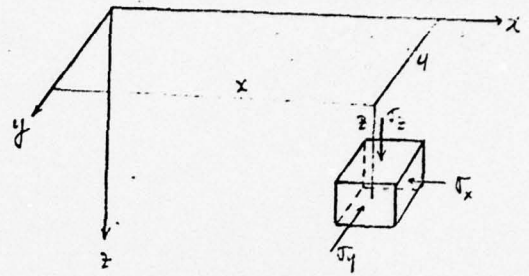
16. Stress conditions. Stresses on an element of soil in cylindrical and rectangular coordinates are shown in figs. 1a and 1b. In an axisymmetric case (fig. 1c), the stress components are independent of the angle θ , and all derivatives with respect to θ vanish. The strains and displacements have the relations

$$\epsilon_r = \frac{\partial u}{\partial r}, \quad \epsilon_\theta = \frac{u}{r}, \quad \epsilon_z = \frac{\partial w}{\partial z} \quad (1)$$

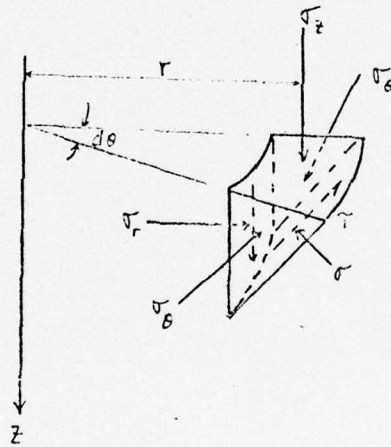
$$\gamma_{rz} = \frac{\partial u}{\partial z} + \frac{\partial w}{\partial r}, \quad \gamma_{y\theta} = \gamma_{\theta z} = 0$$



a. Cylindrical coordinates



b. Rectangular coordinates



c. Stresses on an element in axisymmetric case

Fig. 1. Coordinate systems of stress components

where

$\epsilon_r, \epsilon_\theta, \epsilon_z$ = strains in r, θ , and z directions, respectively

$\gamma_{r\theta}, \gamma_{rz}, \gamma_{\theta z}$ = shear-strain components

u, w = displacements in r and z directions, respectively

17. In the axisymmetric case, displacement in the circumferential direction is zero, since movement is confined to the r-z plane. But strain ϵ_θ in the circumferential direction is not zero and, consequently, stress σ_θ in the same direction exists.

18. In a plane strain case, displacement in the circumferential direction and strain ϵ_y in the longitudinal direction are both zero, but stress σ_y may exist. For the plane strain case, (fig. 1b), equation 1 has the form

$$\epsilon_x = \frac{\partial u}{\partial x}, \epsilon_y = 0, \epsilon_z = \frac{\partial w}{\partial z} \quad (2)$$

$$\gamma_{yz} = \frac{\partial u}{\partial z} + \frac{\partial w}{\partial y}, \gamma_{y\theta} = \gamma_{\theta z} = 0$$

19. In an axisymmetric case, it is possible to determine, by the condition of equilibrium, the normal stress σ and the shear stress τ on the line inclined to the r axis at angle α in terms of $\tau_{rz}, \sigma_r, \sigma_z$, and the angle α (fig. 1c). The equations can be formulated as

$$\sigma = \frac{\sigma_z + \sigma_r}{2} + \frac{\sigma_z - \sigma_r}{2} \cos 2\alpha - \tau_{rz} \sin 2\alpha \quad (3)$$
$$\tau = \frac{\sigma_z - \sigma_r}{2} \sin 2\alpha - \tau_{rz} \cos 2\alpha$$

Stresses on an oblique line in the r-z plane, therefore, do not depend on the circumferential stress σ_θ for the axisymmetric case. It was found that equation 3 is exactly the same for σ and τ in the plane strain state of stress.⁵ Thus, the two-dimensional Mohr circle can be used to represent the state of stress for three-dimensional penetration problems in which the circumferential stress σ_θ can exist but does not influence the normal and shear stresses on the yield surface. The

maximum and minimum principal stresses must lie in the r - z plane for the axially symmetric state of stress since movement is confined to the r - z plane. Thus, σ_θ must be the intermediate principal stress. According to the Harr-Von Karman hypothesis,¹¹ the limiting state of stress at yield is reached when two of the three principal stresses--that is when two Mohr circles--are tangent to the limiting Mohr envelope. Thus, σ_θ must be equal to either the maximum principal stress or the minimum principal stress.

20. Principle of energy conservation. When a probe penetrates the soil at constant speed V , the rate of input energy is RV , where R is the constant resistance experienced by the probe. If it is assumed that the energy RV , which is a function of response behavior of the soil, is totally lost in deforming the soil, the following energy balance equation can be formulated.

$$RV = \int_{\bar{V}} (\sigma_r \dot{\epsilon}_r + \sigma_\theta \dot{\epsilon}_\theta + \sigma_z \dot{\epsilon}_z + \tau_{r\theta} \dot{\gamma}_{r\theta} + \tau_{rz} \dot{\gamma}_{rz} + \tau_{\theta z} \dot{\gamma}_{\theta z}) d\bar{V} \quad (4)$$

The expressions shown at the right are the rates at which the stresses deform the soil medium, and they are integrated over the affected soil volume.

21. In equation 4, the quantities R and V can be measured; and components of rate of strain tensor $\dot{\epsilon}_r$, $\dot{\epsilon}_\theta$, and $\dot{\gamma}_{\theta z}$ can be computed from the velocity field. With appropriate constitutive equations that link soil stresses to strain rates, the components of stress tensor σ_r , σ_θ , $\tau_{\theta z}$, etc., can be obtained in terms of strain rate, and the integration can be carried out. For tests at very slow penetration speeds, the Von Mises equations for perfectly plastic solids were used as the constitutive equation. The results of these tests are presented for future use, and the velocity fields are plotted.

Equations

22. Computation of strain rate fields. For an axisymmetric case,

$$\dot{\epsilon}_r = \frac{\partial v_r}{\partial r}, \quad \dot{\epsilon}_\theta = \frac{v_r}{r}, \quad \dot{\epsilon}_z = \frac{\partial v_z}{\partial z}$$

$$\dot{\gamma}_{rz} = \frac{\partial v_r}{\partial z} + \frac{\partial v_z}{\partial r}$$
(5)

where

$\dot{\epsilon}_r, \dot{\epsilon}_\theta, \dot{\epsilon}_z$ = rates of strain in $r, \theta,$ and z directions, respectively

v_r, v_z = velocities in r and z directions, respectively

$\dot{\gamma}_{rz}$ = rate of shear-strain in r - z direction

For a plane strain case,

$$\dot{\epsilon}_\theta = 0 \quad (6)$$

23. Equations 5 and 6 are valid only for small deformations and are in a strict sense not accurate enough for problems with large strains. However, in view of present crude measuring techniques and other idealization of soil properties, it appears unrealistic to include nonlinear terms in equations 5 and 6 to account for larger strains. Nevertheless, these equations were used for computing strain rates.

24. Levy-Von Mises plasticity equations. The Levy-Von Mises equations are:

$$\begin{aligned} \sigma'_r &= \frac{K\dot{\epsilon}_r}{\sqrt{I}}, \quad \sigma'_\theta = \frac{K\dot{\epsilon}_\theta}{\sqrt{I}}, \quad \sigma'_z = \frac{K\dot{\epsilon}_z}{\sqrt{I}} \\ \tau_{\theta z} &= \frac{K\dot{\gamma}_{\theta z}}{2\sqrt{I}}, \quad \tau_{zr} = \frac{K\dot{\gamma}_{zr}}{2\sqrt{I}}, \quad \tau_{r\theta} = \frac{K\dot{\gamma}_{r\theta}}{2\sqrt{I}} \end{aligned} \quad (7)$$

where

$\sigma'_r, \sigma'_\theta, \sigma'_z$ = stress deviations* in r, θ, z directions, respectively

$$I = 1/2 (\dot{\epsilon}_r^2 + \dot{\epsilon}_\theta^2 + \dot{\epsilon}_z^2) + 1/4 (\dot{\gamma}_{\theta z}^2 + \dot{\gamma}_{zr}^2 + \dot{\gamma}_{r\theta}^2)$$

* It is frequently convenient to decompose the stress tensor into a spherical part corresponding to the mean normal stress and a deviatoric part. The stress deviation is defined as the tensor with the normal components

$$\sigma'_r = \sigma_r - s, \quad \sigma'_\theta = \sigma_\theta - s, \quad \sigma'_z = \sigma_z - s$$

and the same shearing components as the stress tensor. The mean normal stress is defined:

$$s = 1/3 (\sigma_r + \sigma_\theta + \sigma_z) = 1/3 (\sigma_x + \sigma_y + \sigma_z) = 1/3 (\sigma_1 + \sigma_2 + \sigma_3),$$

which is an invariant of the stress tensor.

25. These equations assume that (a) the rate of strain is proportional to the stress deviation, (b) the material is incompressible and nonviscous, and (c) the condition $J_2 = K^2$ is never violated during flow. (J_2 is the second invariant of the stress deviator tensor and K is the yield stress in simple shear.) This last condition implies that work-hardening phenomena do not exist.

26. Since the test soil was near saturation and could be assumed to be incompressible, hydrostatic stresses would not cause any soil straining or energy dissipation, i.e. the hydrostatic stress did not influence the deviatoric stress behavior. Hence, in energy computations, as in equation 4, it was necessary to consider only the deviatoric component of stress, which can be represented by σ'_{ij} , the deviatoric stress tensor.

Material constants

27. In the theoretical analysis of soil mechanics problems, it is very difficult to evaluate the material constants from laboratory test data. These constants depend on a number of factors, probably the most important being the difference in the stress systems, i.e. the laboratory-determined material constants are based on ideal loading conditions that usually do not represent the real conditions under a complex state of stress. If it is assumed that the laboratory triaxial test results can be used to determine soil strength, $K = (\sigma_1 - \sigma_3)/\sqrt{3}$ when the Von Mises yield condition is used. $K = (\sigma_1 - \sigma_2)/2$ when the Tresca yield condition is used.

28. In this study, the Von Mises yield criterion was used. The K value was not determined directly from the triaxial tests, which are difficult and expensive to run at such high moisture contents, but by extrapolations from previous triaxial and cone penetration test results with the same soil. This was done by the following procedure:

- a. Determine the cone penetration resistance of the test soil.
- b. Obtain the value of the cohesion of the test soil from the empirical relation,⁸

$$CI = 12.5 c_t \quad (8)$$

where CI is the cone index of the soil and c_t is the cohesion of the soil determined from triaxial tests, which is equal to $(\sigma_1 - \sigma_3)/2$. (Equation 8 was plotted in pounds per square inch in fig. 5 of reference 11, but may be used for other units.)

c. Compute the K value from $K = 2c_t/\sqrt{3}$.

The penetration resistance of the test soil was found to be 55 kN/m^2 , yielding a cohesion of 4.4 kN/m^3 . K was computed as 5.1 kN/m^2 .

29. Based on results of numerous tests on both fat and lean clays with moisture contents of 45 percent or less (no tests were conducted at 50 percent moisture content comparable to the present study), the relation shown in equation 8 was formulated. Although the error caused by the linear extrapolations beyond the test range is not exactly known, the K value thus obtained should be fairly reasonable. It is very doubtful, however, if this K value is exactly the yield stress that occurred in the soil under penetration.

Laboratory Tests

Soil and its preparation

30. The fat clay used in this study was river alluvium obtained near Vicksburg, Miss., and was classified CH according to the Unified Soil Classification System. Gradation and classification data are shown in fig. 2.

31. The soil was air dried to a uniform moisture content, crushed with a hammer mill, and sieved through a 0.3-cm screen before being mixed with water. The soil and water were thoroughly blended in a pug mill until a uniform consistency was obtained, after which it was stored in an airtight container for about 24 hr before being molded into a sample.

Sample preparation

32. A test sample was prepared in a 50.8-cm-diam mold that could be separated vertically into two halves. Processed soil was compacted in the mold with a mechanically operated, 127-N, wedge-shaped drop hammer falling 15.2 cm. A 1-cm-thick rubber mat was placed over the surface of the soil, but it was lifted occasionally to prevent its sticking to the soil and blocking the free release of air. A sample was made up of 20 layers, each receiving 400 blows of the compaction hammer uniformly over the surface. With this procedure, it is believed that the sample achieved uniformity, and a maximum amount of air was expelled from the soil.

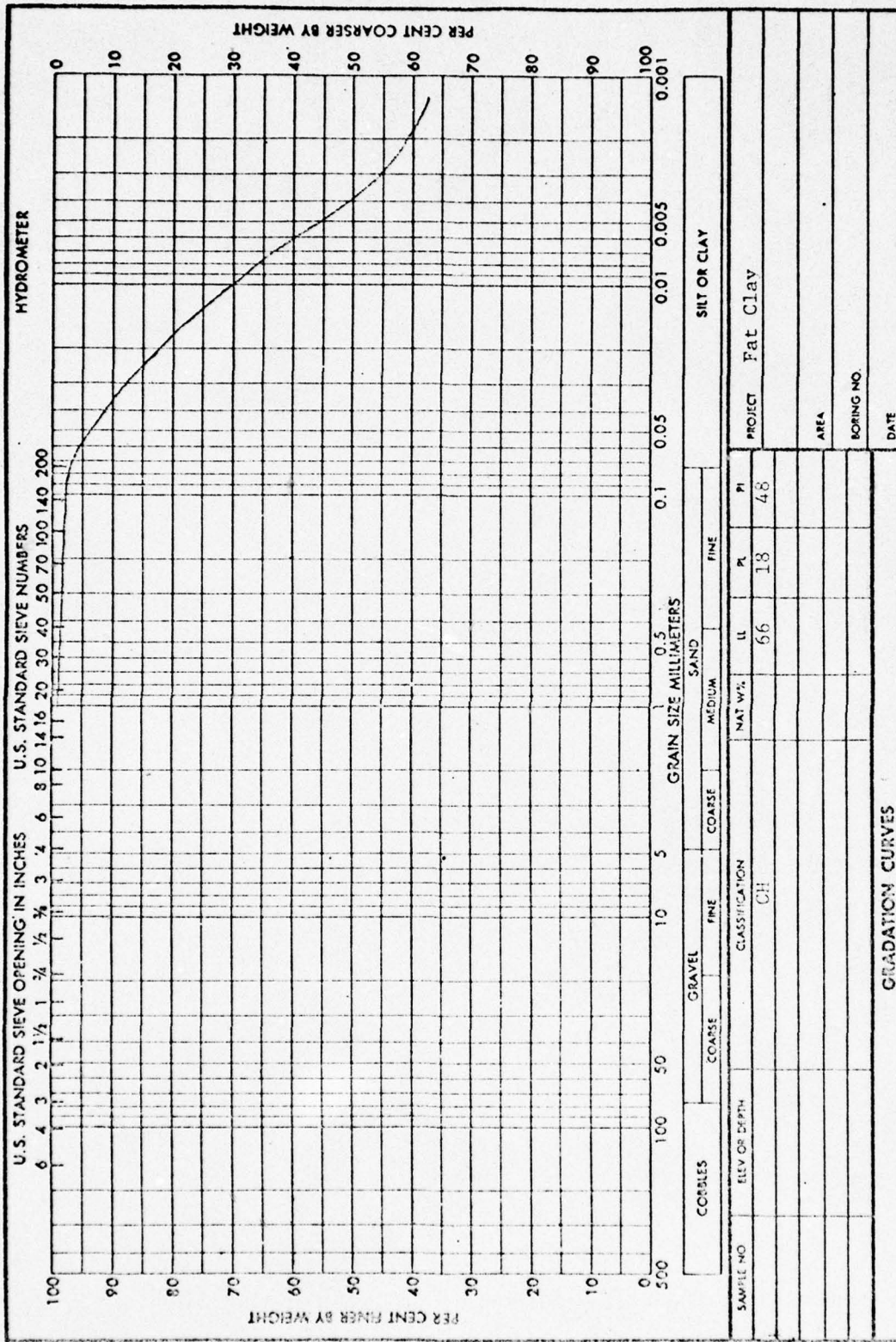


Fig. 2. Soil classification data

Testing procedure

33. After the soil had been compacted, the two halves of the mold were slightly disengaged, and the sample was cut vertically in half with a piano wire. The mold was disassembled and laid on a table with the flat soil surface up.

34. Straight, orthogonal grid lines were drawn at 1.27-cm intervals on the soil surface with a sharp pencil. At locations where the grid lines would be destroyed by penetration, small colored pins were inserted. The complete pattern of the grid lines then was traced on a transparent plastic sheet. After the soil surfaces were oiled lightly, the two halves of the mold were put back together, and the penetration tests were made near the center of the mold.

35. After penetration, the mold was disassembled and the halves were separated again. The deformation pattern of the grid lines was traced on the same plastic sheet.* Where the lines were destroyed by penetration, the areas could be reconstructed readily by the new positions of the colored pins.

Accuracy of test method

36. The test method used in this study was rather crude. Factors that affected the reproducibility of test results were found to be:

- a. Variation (within ± 2 percent) in moisture content of the samples.
- b. Nonuniformity of the samples.
- c. Variation in the penetration technique (i.e. a slight eccentricity of the penetration could not always be avoided).

In two different soil samples prepared and penetrated under identical conditions, the penetration resistance values were very close, but the deformed grid lines (or the soil flow patterns) were not exactly the same. In other words, the displacement of a soil particle at a particular location in one soil sample was not the same as in the same location in a second sample. However, this did not seem to constitute a problem in this study, because the computations were based on integration over the total volume of the

* In both axisymmetric and plane strain cases, soil particles moved only in the cut plane.

deformed soil and did not depend on individual particle movements.

Presentation of Test Results and Their Analysis

37. The results of this study are presented in three parts: (a) laboratory test results that show the flow characteristics and particle movement of the soil under penetrations, (b) the computer program, and (c) the theoretical prediction of penetration resistance. The penetration resistance was predicted by assuming the deformation energy of the soil to be equal to the penetration energy, and an integration of the deformation energy over the total affected volume of the deformed soil was carried out to obtain the penetration resistance. The computed penetration resistance then was compared to the measured cone penetration resistance.

Laboratory test results

38. Representative laboratory test results are shown in table 1 and plates 1-10. Nonhomogeneity of the test soils could not always be avoided, so the deformation patterns on opposite sides of the probe were usually dissimilar. This was reasonable because the load tended to deform most on the side that offered the least resistance. Occasionally, the magnitude of displacement at a distant point was found to be greater than that at a point closer to the probe.

39. Test results for a 30-deg circular cone with a base area of 2.3 cm^2 (5.4 cm in diameter) are presented in plates 1-4. Penetration speed was 5.6 cm/sec, the highest used. (The pins near the cone in plate 1 were placed after the test to provide a better contrast in the photograph; this was found later to be unnecessary.) The affected zone was rather small, and soil beneath the tip of the cone seems not even to have moved. The stream lines (flow paths) of soil particles are shown in plate 2. Plate 3 is the complete trace of soil particle movements at the grid points from the time when the cone was just touching the soil surface until the end of the test.* The displacement vectors of soil of soil particles at grid points around the cone are presented in plate 4;

* This result was obtained by assumption of steady state, which is discussed in paragraph 45.

the starting and ending points of each arrow show the original and final positions of the soil particles.

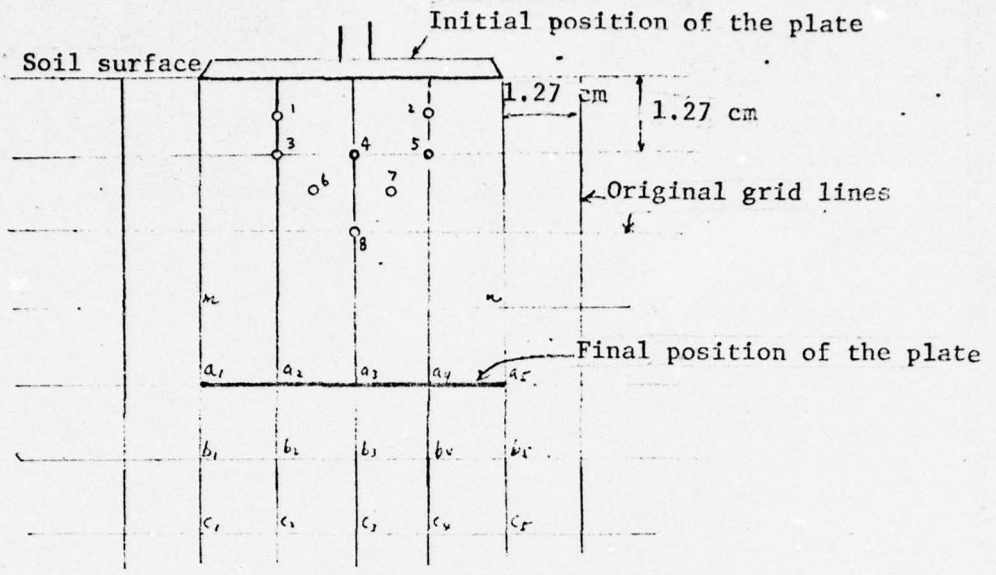
40. Results of tests with a 5.1-cm-diam circular plate moving at an extremely slow speed (0.004 cm/sec) are presented in plates 5-7, and with a 3.8- by 22.8-cm rectangular plate at the same speed in plates 8-10. (The pins shown in plates 5 and 8 were placed before the tests.) Under this slow penetration speed, the soil was generally assumed to behave as a perfectly plastic material, an assumption that did not necessarily apply to fast penetration speeds.

41. The portion of soil that moved with each plate is termed the soil nose in this report. Soil noses under the circular plate penetrating at four different speeds are shown in figs. 3b-3c, and under the 5.1- by 25.4-cm rectangular plate at two different speeds in figs. 4b and 4c. Figures 3a and 4a show the locations of pellets embedded in the soil and the original grid lines before penetration. The soil nose formed under the 5.1- by 25.4-cm rectangular plate by penetration at a very slow penetration speed (fig. 4b) had a triangular shape, but changed to circular as the speed was increased to the standard 3.1 cm/sec (fig. 4c).

42. Soils in the vicinity of the soil noses experienced large shear strains. Because of the adhesion force between the plates and the soil, the portion of soil near the plates did not move away, but moved vertically downward with the plate like a rigid body. This may be verified by the position (relative to the plate) of pellet No. 4, which was 1.27 cm below the center of the plate before and after penetration in all tests. Pellet No. 1 did not move away in any of the tests; pellet No. 2 moved slightly in some tests in which the soil conditions on the right side of the mold were apparently weaker than on the left. Pellet No. 8, which was placed at a depth half the width of the plate (2.54 cm) below the center of the plate, was lost in most tests.

43. Deformation patterns were distinctly different in cases of plane strain and axisymmetry. In the plane strain case (plates 8, 9, and 10*), the deformations were extended to a large area; the soils along the edge

* These tests with an elongated plate (3.8 by 22.8 cm) can be considered plane strain tests.



a. Locations of embedded pellets

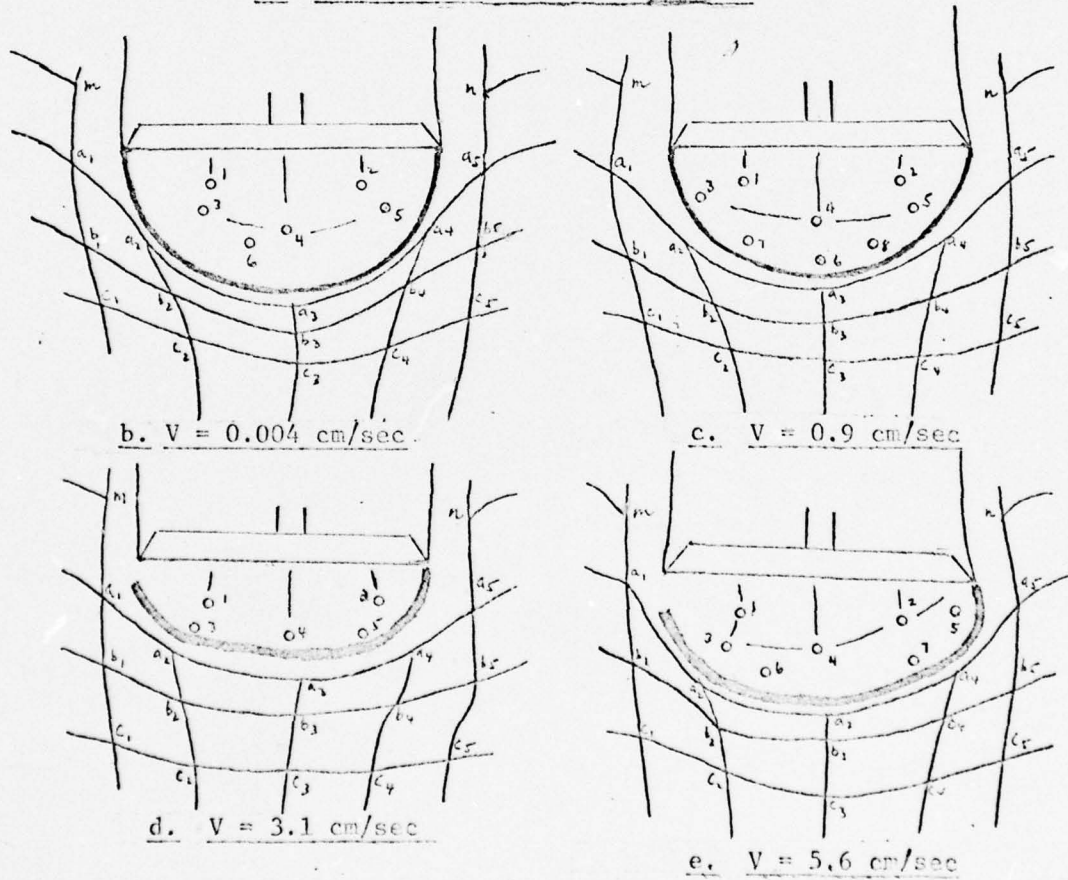


Fig. 3. Soil noses beneath a 5.1-cm-diam circular plate at various penetration velocities

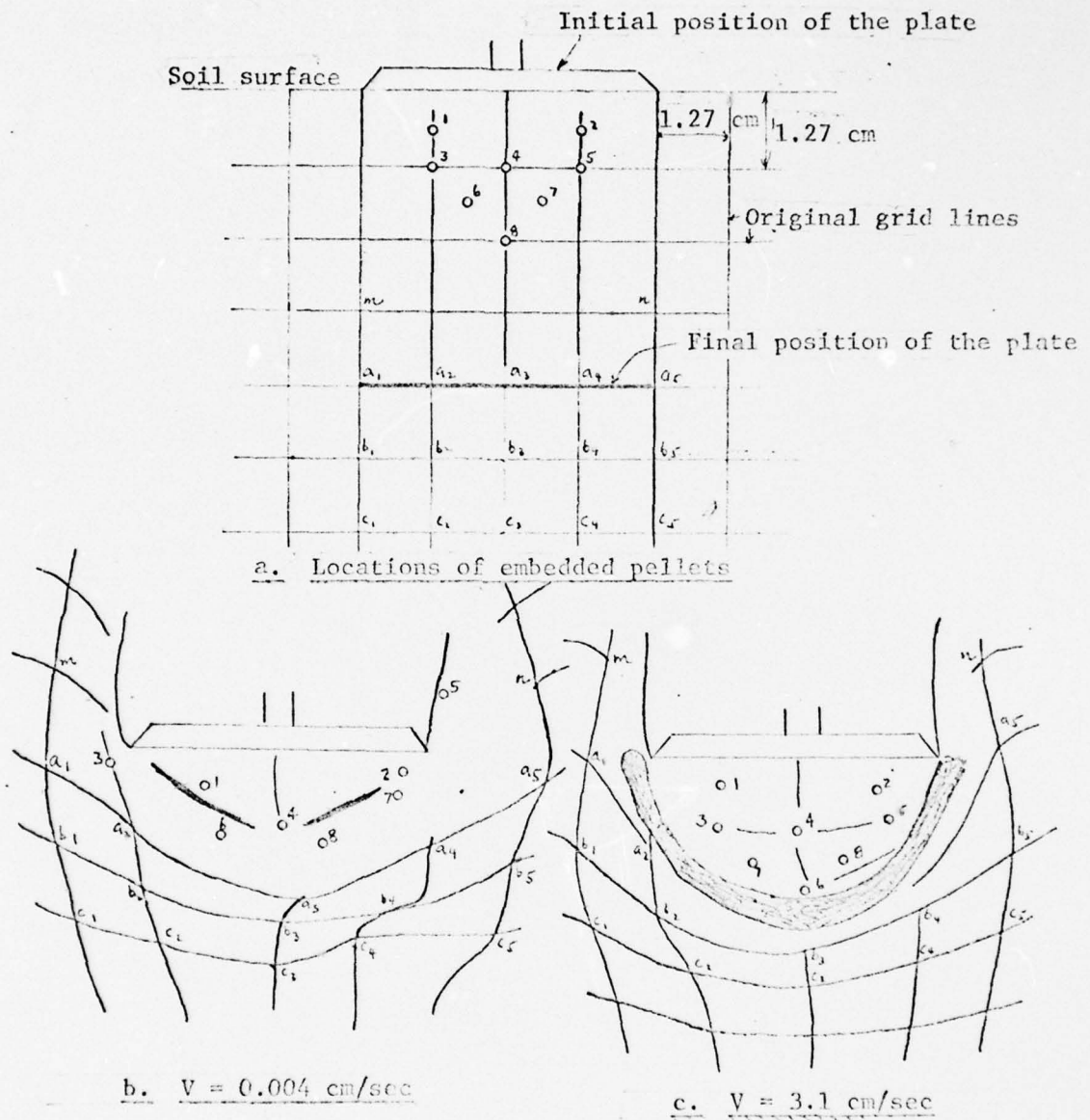


Fig. 4. Soil noses beneath a 5.1- by 25.4-cm rectangular plate at two different penetration velocities

of the mold were heaved slightly, indicating the mold actually was not large enough for the deformation patterns to be complete. The soil evidently was failed by shear stresses, the failure lines showing clearly in plate 8. Although the soil was failed by shear stresses in the axisymmetric case (plates 5 and 7), no rupture lines can be seen. This soil responded to penetration as viscous fluids might, and the soil deformations were limited to small areas near the plate. Despite these differences, the unit penetration resistances for these cases were not very different from each other, as shown in table 1. When the flow patterns in plates 1 and 5 are compared, it can be seen that penetration speed had no effect on soil deformation patterns in the axisymmetric case. In the plane strain case, however, the failure lines are still seen at a penetration speed of 3.1 cm/sec, but not as clearly as at slower penetration speeds.

44. The soil flow patterns in the zone near the penetration hole were not exact because the soil here tended to flow toward the hole by gravity. This lateral soil movement occurring during and after the penetration gave false information for computed results of strain rate fields. The magnitude of this error, however, could hardly be evaluated.

45. To trace the continuous movements of soil particles under penetration, the deformed grid lines are recorded as a function of time. This can be done by: (a) the X-ray method used by Yong¹⁰ and Miller,⁶ and (b) the measurement of deformed grid patterns in identical soil samples penetrated at different depths. The first method could not be used for this study because X-ray facilities for testing large samples were not available at the WES. The second method was not used because a large number of tests are required, and identical soil samples are very difficult to prepare. Instead, steady state of movement of soil particles was assumed; this allowed the continuous soil particle movement to be deduced from the final positions of the deformed grid lines. Actually, the validity of the use of the superposition technique to trace the entire history of soil particle movements is thus assumed.

46. The grid lines in a test sample being penetrated by a cone are shown schematically in fig. 5. The horizontal lines before penetration are shown in fig. 5a, and the deformed patterns at successive times in figs. 5b, 5c, and 5d. Under assumed steady state, line 3-d should have

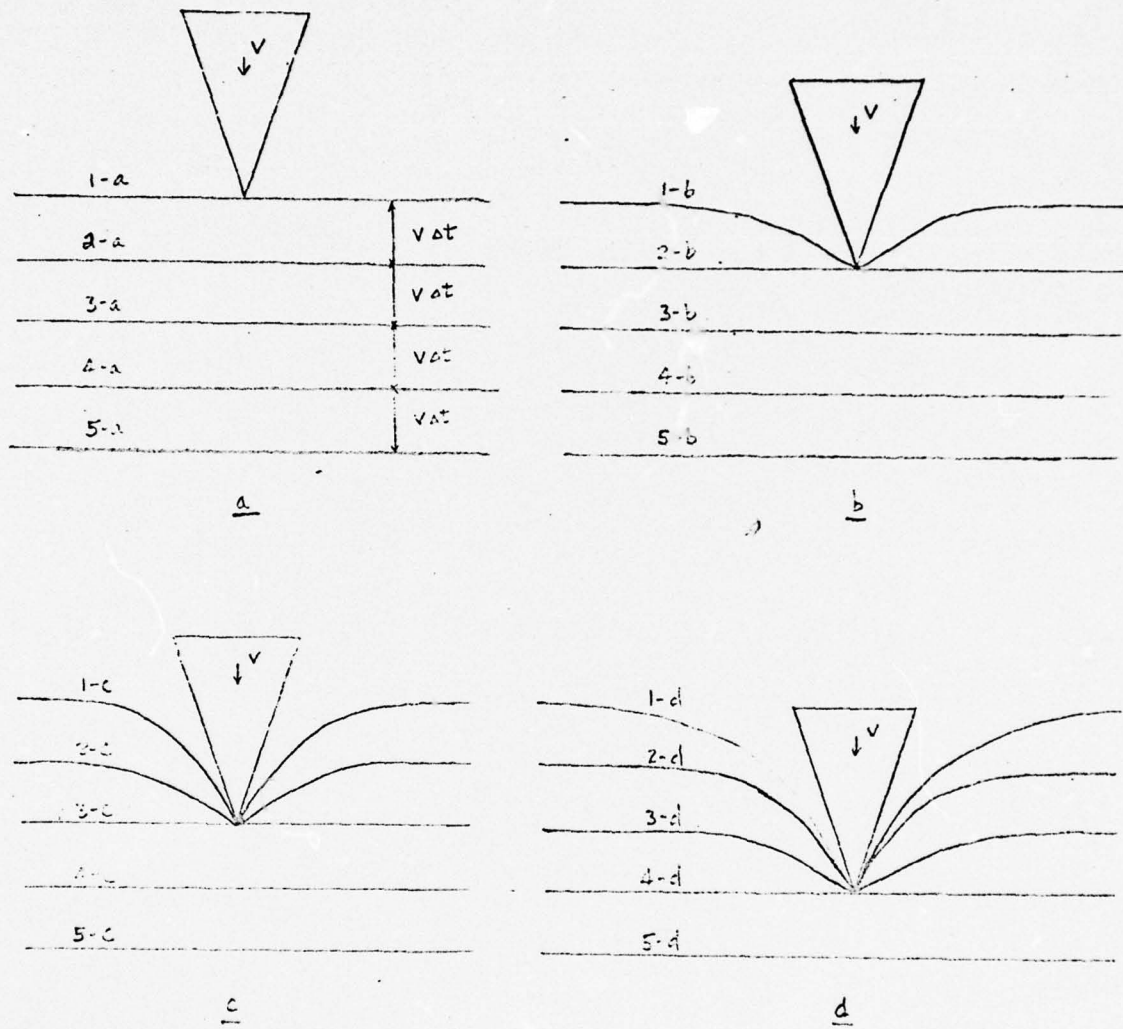


Fig. 5. Steady-state penetration of soil sample

the same shape as lines 2-c and 1-b; also, line 2-d should have the same shape as line 1-c. As the cone penetrates further into the soil, the deformed lines surrounding the cone should have the same shape as those at Δt time ago. In other words, the patterns of deformed lines are independent of depth, just as the waves surrounding a sailboat do not change as long as the boat is moving at constant speed.

47. Experimental results obtained at the WES⁸ have shown that penetration resistance of clay does not depend upon penetration depth, except for small variation due to overburden. The strength of the soil surrounding the probe does not change as the probe penetrates the soil so the soil can be assumed to be a uniform and homogeneous medium with constant strength. Hence, the assumption of steady state for the cases investigated herein seems to be valid.

Computer program and results

48. A computer program (Appendix A) was prepared to be used for predicting penetration resistance of the soil. It was written in three parts:

- a. Computation of velocity field.
- b. Computation of strain rates at grid points.
- c. Computation by the Von Mises equation of the stress components at each grid point and the rate of stresses deforming the soil

Based on the energy balance equation 4, the validity of the Von Mises equation was checked. The numerical value of soil yield stress was determined by laboratory triaxial tests previously conducted.

49. The essential work in the program was to compute the strain rates at the grid points. Equations 5 and 7 were used for this purpose with the input data measured from test results.

50. The original grid lines (solid) and the stream lines (dashed) are shown in fig. 6a; fig. 6b shows the complete trace of soil particle movement at each grid point, from time $t = 0$ to $t = 5\Delta t$ where Δt is the time required for the cone to move through the distance D . The displacements in r and z directions, as a function of time t , are presented in figs. 6c and 6d, respectively. There are various ways to compute the velocity field and strain rate field. That used to compute a velocity field is as follows:

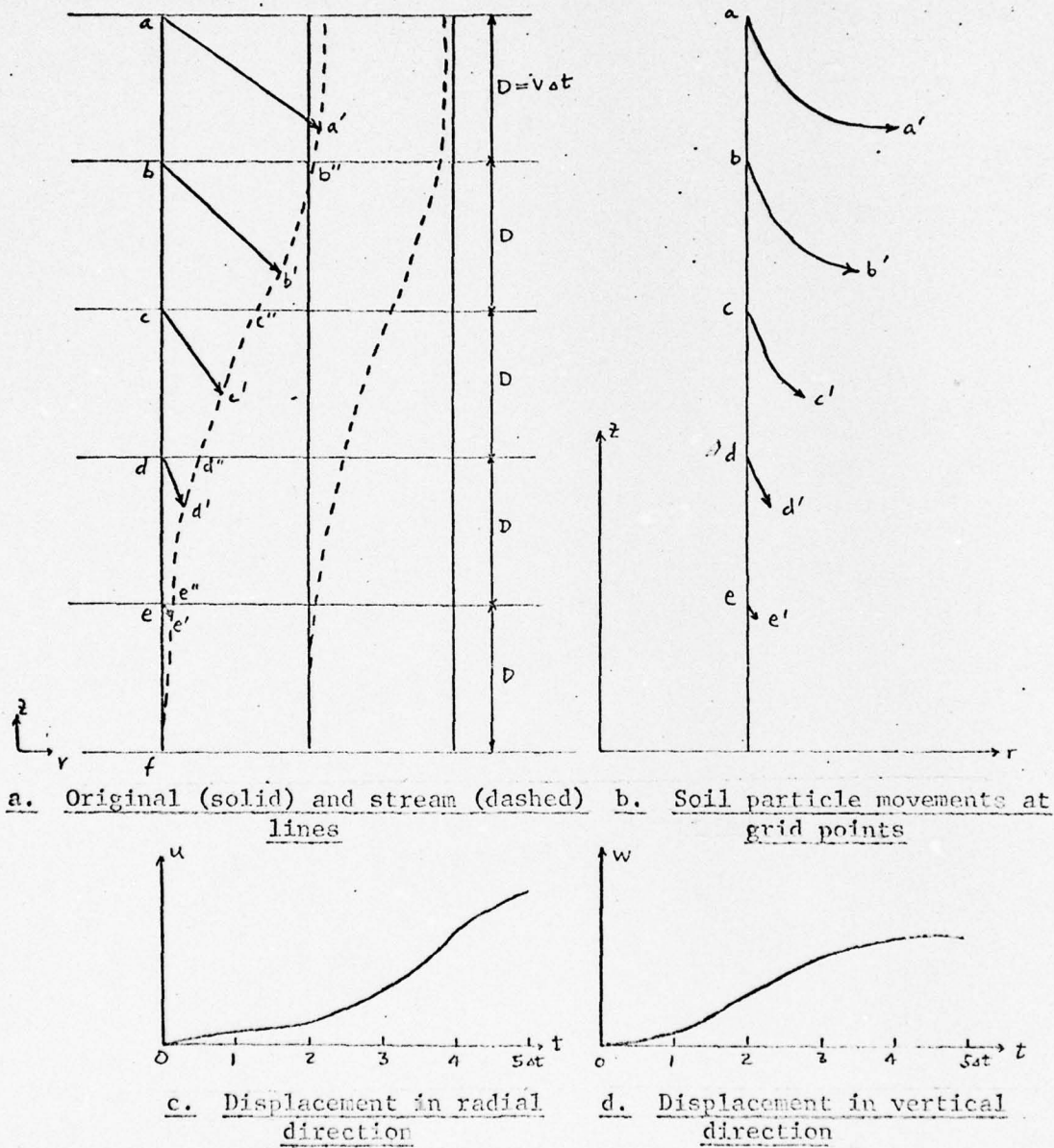


Fig. 6. Data reduction

- a. The locations of deformed grid points, i.e. a' , b' , c' , d' , e' , and f' (fig. 6a), were first read into the computer. The measurements were taken with reference to a fixed coordinate system.
- b. The displacements u and w were computed according to the definition $(u \text{ or } w)_{t_0 \rightarrow t} = \text{total displacement up to time } t \text{ minus displacement at time } t_0$.
- c. An n -th order polynomial based on the least square technique was generated by the computer and represented the displacement versus time curves. The slopes of the curves at time $t = \Delta t$, $2\Delta t$, $3\Delta t$, $4\Delta t$, and $5\Delta t$ resulted in velocities corresponding to points e' , d' , c' , b' and a' , respectively (fig. 6a). It was found that polynomials with an order of 8 would fit most data with an acceptable degree of accuracy.

51. To compute a strain rate field, the following steps were taken:

- a. Based on values of velocities at points a' , b' , c' , d' , and e' along a stream line, velocities at points b'' , c'' , d'' , and e'' were obtained. These points were actually the intercepts of the stream line on the undeformed horizontal grid lines.
- b. After these velocities had been obtained for all stream lines, the velocities at each intersection on the undeformed grid were generated by the computer, and the horizontal and vertical components of the velocities, as well as the rate of change of velocities in both directions, were determined by the least square method in conjunction with polynomials. Thus, the strain rate tensor $\dot{\epsilon}_{ij}$ at each grid point was obtained.

52. Difficulty was encountered, however, in using the least square procedure in paragraph 51b. According to computer print-outs, velocities did not always increase or decrease monotonically, but fluctuated in one direction. For example, velocities along a vertical grid line below the probe did not always decrease with depth. It was found that the variation in the order of polynomials was very sensitive to the variation in velocity values. The correct order for a given set of data could not be determined analytically by any method except trying a series of different values. In this program, orders from 3 to 14 (less than the data points) were tried, and the one that gave the best approximation was selected in the computation.

53. A velocity field shows the flow pattern of soil under

penetration. The velocity fields beneath probes at the moment penetrations were completed are depicted in plates 11-16. (Since steady-state conditions were assumed, the same velocity field should be observed at any other stage of penetration.) The arrows shown indicate the magnitude of velocity and direction of movement of soil particles, and the dashed lines show the stream lines. These lines indicate the directions of maximum shear stress.⁷ Along the stream lines, velocities of soil particles were relatively large close to the probe, but became smaller as the distance increased from the probe. In other words, the velocity decreased along each stream line. The rates of change of velocity (or strain rate) along the stream lines at slow penetration speed (plates 11, 13, and 15) were observed to be smaller than those at faster penetration speeds (plates 12, 14, and 16). Since the deviatoric stress is proportional to the strain rate, according to the Von Mises concept, the stresses along equivalent stream lines should be greater under faster penetrations than under slower ones. This is reasonable because experimental results revealed that the penetration resistance increased with increasing penetration speed.

54. It is interesting to note that soils under penetration do not move along a unique slip surface in the velocity fields as most theoretical analyses have assumed (fig. 7). It usually is assumed that at the time of

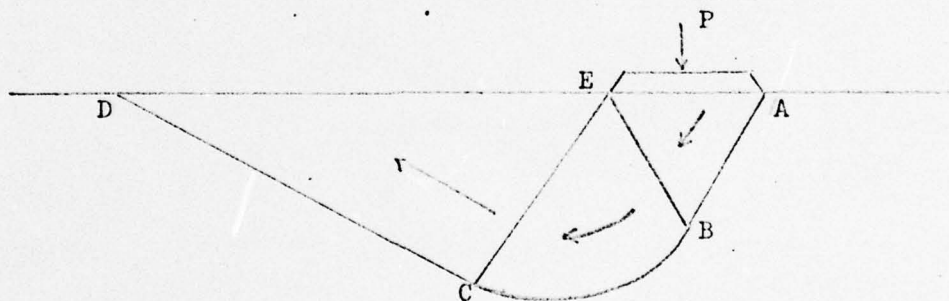


Fig. 7. Soil movements beneath a footing

failure, soils beneath the failure surface ABCD do not move at all, while soil masses in portions ABE and ECD slide to the left like a rigid body along surface ABCD without internal energy dissipation. Energy is dissipated along the surface ABCD and within the fan BCE. This was not

the case, however, for the cases in this study: The velocity varied along the stream line and also among stream lines; also, the grid squares were distorted after movement (plates 1, 5, and 8), indicating that there were relative displacements among soil particles that moved along infinite numbers of surfaces rather than along a unique surface.

55. It is important to realize that the assumption of rigid body movement of a soil mass beneath a footing applies to the condition of incipient failure or limit equilibrium, i.e. the initial movement of the soil mass at the beginning moment of failure. With continued movement, as in this study, the soil mass may deviate from the simple rigid body.

56. The computed velocity field beneath a 3.8- by 22.8-cm rectangular plate moving downward at a very slow speed (0.004 cm/sec) (plate 15) can be compared with the rupture lines in the soil sample after the test (plate 8). It appears that the computed directions of soil particle movement checked quite well with the observed direction or rupture lines, indicating that the computation method for velocity fields employed in this study was reasonably accurate.

57. In the velocity field beneath a 5.1- by 25.4-cm rectangular plate moving downward at a speed of 3.1 cm/sec (plate 16), the stream lines (velocity field) appear to be different from those in plate 15. At slow penetration speed (plate 15), the soils moved away from the probe in a markedly horizontal direction; whereas at faster speed (plate 16), soil near the probe moved in a markedly vertical direction.

58. Velocity fields beneath a 5.1-cm-diam circular plate at penetrating speeds of 0.004 and 5.6 cm/sec are shown in plates 13 and 14, respectively. The velocity fields differed under these two speeds, as did those in plates 15 and 16, and the same discussions apply. As the penetration speed increased, the stream lines generally became steeper, and the distance from the probe to the ends of the flow lines decreased.

59. Plates 11 and 12 are similar to plates 13 and 14, except that a 5.4-cm circular cone was used. Because of the sharp apex angle of the cone, soils beneath the cone tip were hardly moved. Otherwise, the discussions previously made for other types of probe are also applicable to results with this one.

Theoretical prediction
of penetration resistance

60. The procedure for computing the penetration resistance based on the measured strain rate fields is given in this section. The computer results were limited to the axisymmetric cases at very slow penetration speeds (Nos. 1 and 2 in table 1).

61. With the velocity components at each grid point known, the components of strain rate can be computed; with the proper constitutive equation for the soil, the total resistance of the soil can be evaluated by equation 4 (the energy balance equation) and theoretically should be equal to the measured penetration resistance. In using equation 4 to carry out the integration, only the affected soil volume beneath the probe was considered; the effect of soil above the probe was discarded. This simplification was assumed as a direct consequence of the steady-state assumption; it reduced the effect of the soil above the probe to simple overburden pressure, which was insignificant in the investigated cases since the penetration resistance in clay remained almost constant after full penetration of the probe. Also, the soil above the probe tended to move toward the penetration hole, resulting in unrealistic and false velocity and strain rate fields insofar as the prediction of penetration resistance was concerned.

62. To save computer time, it was assumed that the deformation energy in the soil under penetration was symmetrical with respect to the probe. Consequently, the computations were carried out for one half of the mold only. In the analysis, the Levy-Von Mises plasticity equation was used. The soil yield stress K was taken as 5.1 kN/m^2 (paragraph 28). The soil resistances computed from the measured strain rate fields were very much larger than the measured penetration resistances, as shown in the following tabulation.

Test No.	Probe	Penetration Speed cm/sec	Measured Resistance N	Computed Resistance N	Computed Soil Yield Stress K kN/m ²
1	5.1-cm circular plate	0.004	110 ✓	680	0.76
2	5.4-cm circular cone	0.004	133 ✓	431	1.53

63. If the theory of plasticity is assumed to be valid for frictionless materials, and if the measuring technique and the computed strain rates are assumed to be reasonably accurate, questions may arise as to whether the numerical value of soil yield stress K used in computations is properly chosen. In the Levy-Von Mises equation, K is defined as the yield stress in shear, or $1/\sqrt{3}$ yield stress in tension or compression. It is, of course, questionable whether the yield stress determined from the laboratory triaxial test can represent the yield stress under the complex state of stress in the soil sample under penetration. If the computation including the simplifying assumptions is reasonable, the real soil yield stress K under penetration may be computed by equation 4. Substituting the Levy-Von Mises plasticity equation 6 into equation 4 yields

$$RV = K \int_{\bar{V}} (\dot{\epsilon}_r^2 + \dot{\epsilon}_\theta^2 + \dot{\epsilon}_z^2 + \frac{1}{2} \dot{\gamma}_{rz} + \frac{1}{\sqrt{I}}) d\bar{V} \quad (9)$$

Since R and V are measured and the components of the strain rate tensor can be computed, the soil yield stress K under penetration can be computed from equation 9. These values are listed in the last column of the tabulation in paragraph 62.

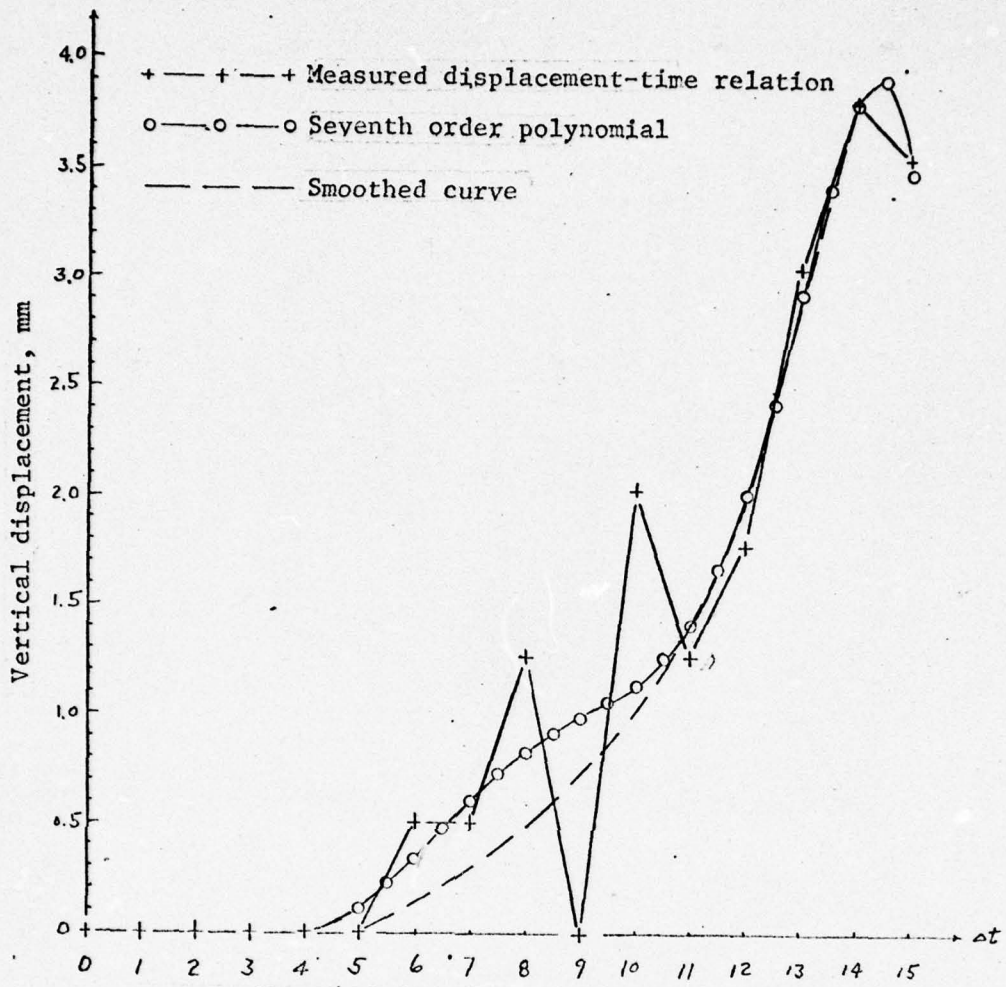
64. The large discrepancies between the measured and computed penetration resistance values in these two tests may be explained by:

- a. The soil was nonuniform, i.e. the deformation patterns at the cut surface did not well represent those on other surfaces.
- b. The Levy-Von Mises equation was inadequate for describing the soil behavior under penetration, i.e. according to the Von Mises equation, it is reasonable to believe that the rate of strain is proportional to the stress deviation during flow, but it is questionable whether the yield condition $J_2 = K^2$ is always valid during flow. Also, the soil samples were not exactly incompressible, which violates the basic assumption of Von Mises equation.
- c. Errors were caused by the high-order polynomial approximations, i.e. in the computer calculations, the measured displacement data were fed into the computer without first being smoothed. A polynomial with higher order was desirable to approximate the relation of displacement to time. Although a high-order polynomial may be able to approximate the displacement-time relations with fair precision, the

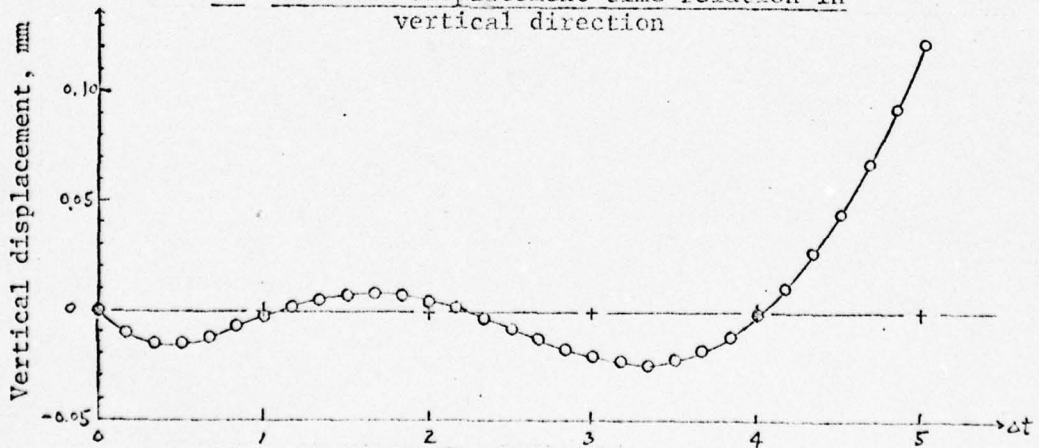
derivatives of the polynomial would deviate very much from those of the displacement-time relation due to the oscillating nature of the high-order polynomial. This may best be explained by an example. The solid line connected by crosses in fig. 8a shows the measured displacement-time relation of a soil particle in the vertical direction. A seventh-order polynomial was generated based on these data points and was plotted in the line connected with circles. The portion of the curve between time 0 to time $5\Delta t$ is plotted at an enlarged scale in fig. 8b. The horizontal line was actually approximated by an oscillating curve with the difference less than 0.023 mm. When the derivatives of the polynomial were taken at various times, however, the values were not zero. As a result, nonzero velocities or nonzero strain rates existed in this time interval. In other words, positive deformation energy was computed in the portion of the soil in which measured soil movements were actually zero. The deformation energy was always positive because the components of the strain rate tensor in equation 9 were squared before summing for every small soil volume. In some cases, when the soil particles were undergoing rigid-body movements, i.e. the soil particles moved at constant velocity without interval energy dissipation, positive deformation energy would be computed for the same reason described above.

Among all these reasons, it is believed that the errors caused by high-order polynomial approximations were most serious. To overcome this difficulty, the computer program can be modified as described below.

65. The measured displacements should be smoothed before being fed into the computer. (The dashed line in fig. 8a is a smoothed displacement-time curve.) In the time interval between zero and $5\Delta t$, the velocities would be assumed equal to zero. A polynomial with very low order or a simple function would be accurate enough to approximate this displacement-time curve without oscillation. It should be pointed out that the soil displacements were actually very small, the differences between the smooth curve and actual measurements were less than 1 mm. In fact, measurements less than 1 mm were determined quite arbitrarily. It is reasonable to believe that the smoothed curve would better represent the real displacement-time relations of the soil particles, since the soil sample could be considered a continuous medium.



a. Measured displacement-time relation in vertical direction



b. Enlarged portion of a above

Fig. 8. Displacement-time curves

Conclusions

66. Based on the test data and computer results, it is concluded that:
- a. The soil patterns under penetration can be drawn based on the measured soil particle movements (paragraphs 50-59).
 - b. The soil flow patterns in two-dimensional, plane strain cases are different from those in axisymmetric cases. In both cases, the shape of the stream (or flow) lines change with change in penetration speeds. In general, at the high penetration speeds of this study, the rate of change in the slope of the stream lines is greater and the distances from the ends of the stream lines to the probe become smaller than at slow speeds. Also, at the high penetration speeds, the rate of velocity change (or strain rate) along stream lines is greater; stresses in the soil are consequently greater to counterbalance the higher penetration force (paragraph 53).
 - c. The clay beneath the moving probe does not move entirely as a rigid body along a unique failure surface; rather it moves along infinite numbers of failure surfaces (paragraph 54).
 - d. The penetration resistances computed from measured soil movements are larger than measured values, indicating the possibility that the soil constant determined from triaxial tests may not represent the real soil strength under penetration (paragraphs 62 and 63).
 - e. The apparent discrepancy between computed and measured penetration resistance suggests that the usual mathematical procedure, which tends to magnify the errors inherent in the basic test data, is not appropriate for the problem of soil-vehicle interaction, unless an objective method to smooth the experimental curves is developed (paragraphs 64 and 65).

Literature Cited

1. Christian, J. T., "Two-Dimensional Analysis of Stress and Strain in Soils; Plane-Strain Deformation Analysis of Soil," Contract Report No. 3-129, Report 3, Dec 1966, U. S. Army Engineer Waterways Experiment Station, CE, Vicksburg, Miss.
2. Drucker, D. C., "A More Fundamental Approach to Plastic Stress-Strain Relations," Proceedings, First U. S. National Congress on Applied Mechanics, 1951, pp 487-491.
3. Drucker, D. C. and Prager, W., "Soil Mechanics and Plastic Analyses or Limit Design," Quarterly of Applied Mathematics, Vol 10, 1952, pp 157-175.
4. Drucker, D. C., Gibson, R. E., and Henkel, P. I., "Soil Mechanics and Work-Hardening Theories of Plasticity," Transactions, American Society of Civil Engineers, Vol 122, 1957, pp 338-346.
5. Jumikis, A. R., Mechanics of Soils, Van Nostrand, Princeton, N. J., 1964, p 14.
6. Miller, P. M., "A Report on the Application of the Visioplasticity Method to Soft-Soil Mobility Problems," Technical Memorandum No. VJ-2330-G-53, 1968, Cornell Aeronautical Laboratory, Inc., Buffalo, N. Y.
7. Prager, W. and Hodge, P. G., Theory of Perfectly Plastic Solids, Wiley, N. Y., 1951, p 143.
8. Smith, J. L., "Strength-Moisture-Density Relations of Fine-Grained Soils in Vehicle Mobility Research," Technical Report No. 3-639, Jan 1964, U. S. Army Engineer Waterways Experiment Station, CE, Vicksburg, Miss.
9. Whitman, R. V., "Multidimensional Analysis of Stress and Strain in Soils," DASA No. 1558, 1964, Defense Atomic Support Agency, Washington, D. C.; prepared by Stanford Research Institute, Menlo Park, Calif.
10. Yong, R. N. and Webb, G. L., "Energy Considerations in Wheel-Clay Soil Interaction," Report No. DR EO 32 (Geophysics), June 1969, Soil Mechanics Series, McGill University, Montreal, Canada.
11. Zadnek, S., "The Slip Lines and Slip Surfaces in the Theory of Plasticity and Soil Mechanics," Applied Mechanics Review, Vol 15, 1961, p 753.

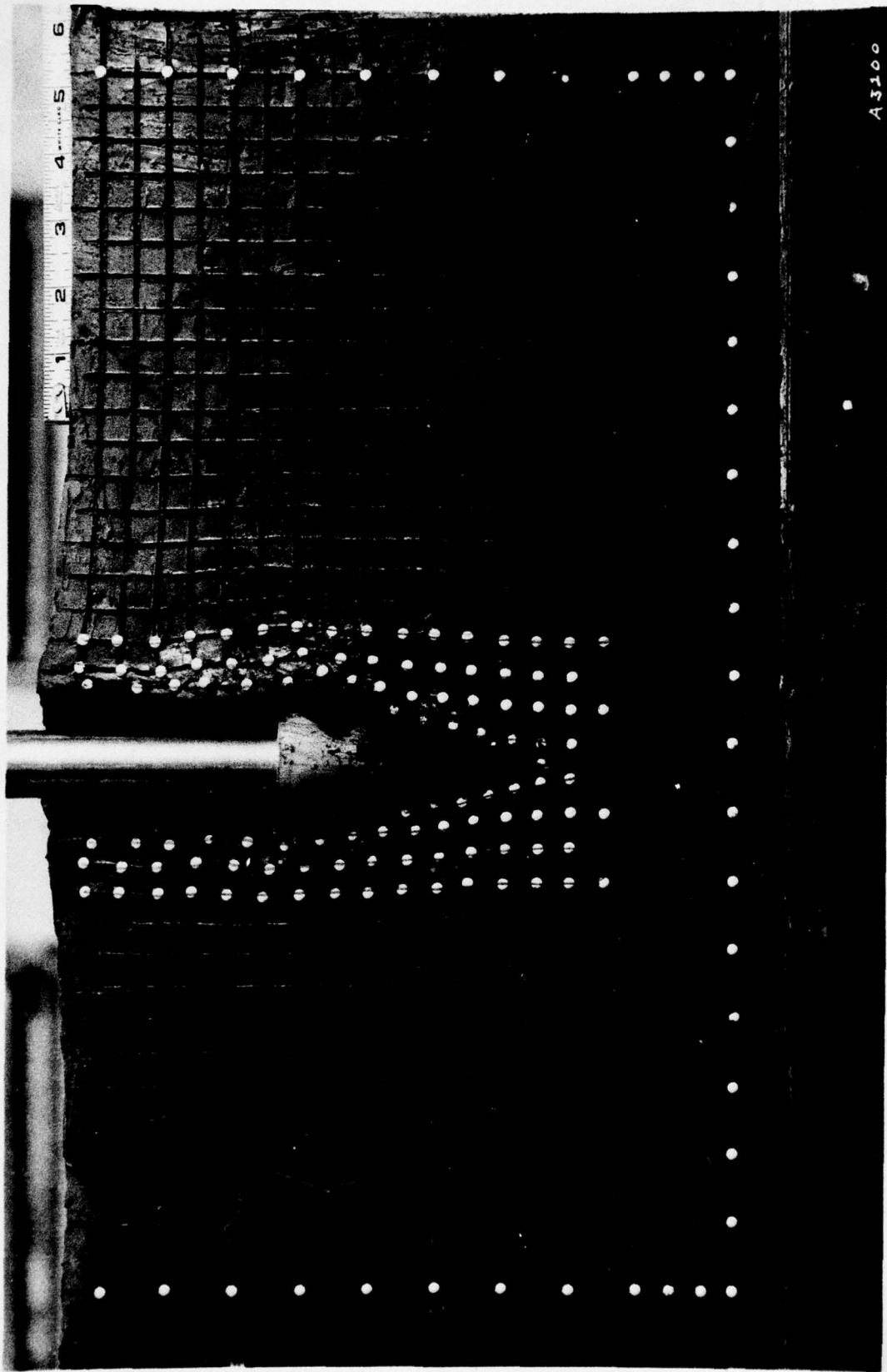
Reproduced from
best available copy.



Table 1

Laboratory Soil Sample Data

Test No.	Penetrometer		Moisture Content %	Saturation %	Resistance	
	Type	Speed cm/sec			Total N	Unit kN/m ²
1	5.1-cm circular plate	0.004	49.1	97.5	110	54.2
2	5.4-cm circular cone	0.004	50.6	97.5	133	57.6
3	3.8- by 22.8-cm plate	0.004	51.7	99.0	350	40.2
4	5.1- by 25.4-cm plate	0.004	49.5	97.0	501	38.8
5	5.1- by 25.4-cm plate	3.0	49.7	99.0	750	58.6
6	5.1-cm circular plate	0.9	50.8	99.0	120	59.2
7	5.1-cm circular plate	3.0	49.9	97.5	140	68.9
8	5.1-cm circular plate	5.6	51.2	97.0	240	118.5
9	5.4-cm circular cone	0.9	51.8	99.0	160	68.9
10	5.4-cm circular cone	5.6	50.0	97.0	300	129.5



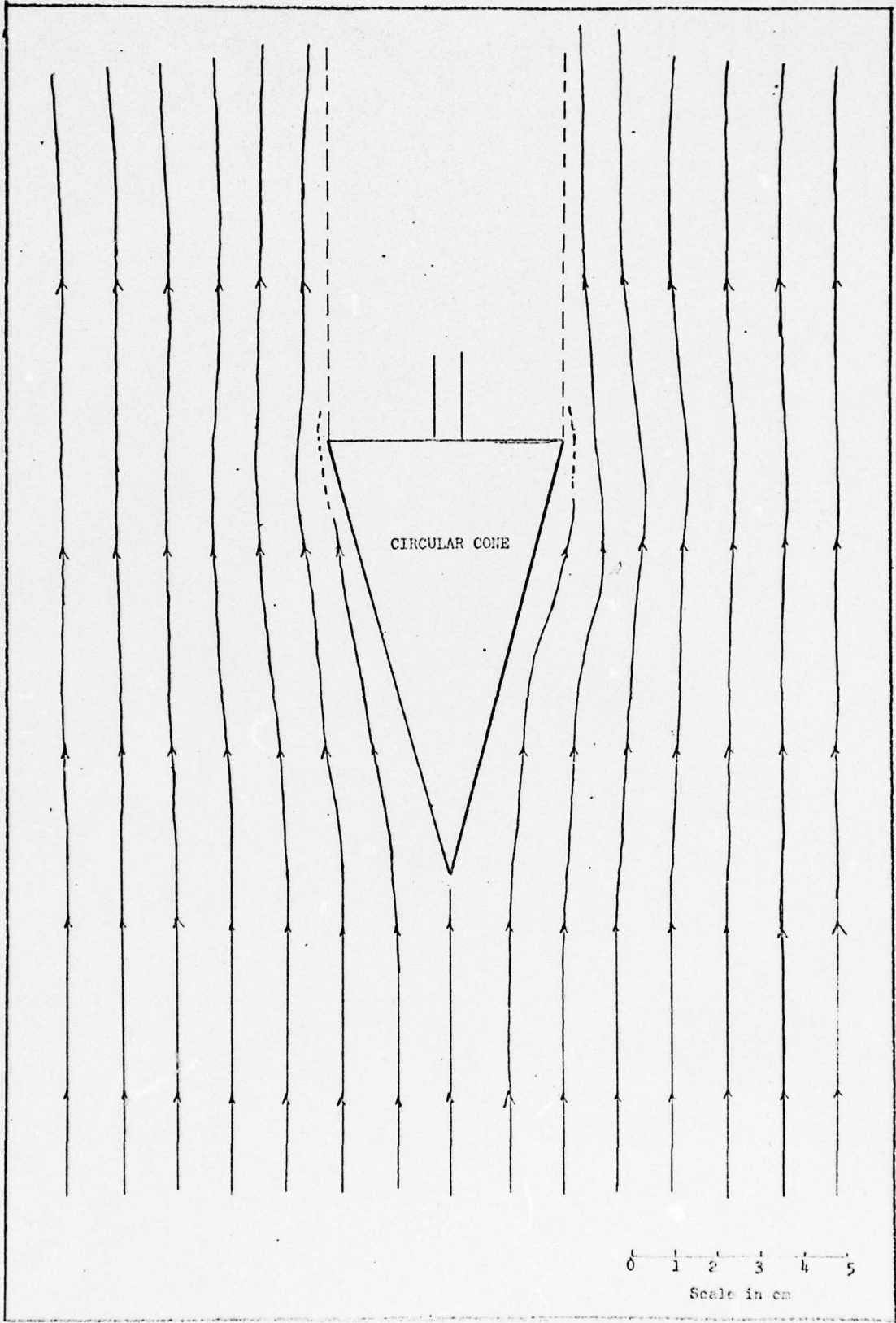
A3100

SOIL FLOW PATTERN AFTER PENETRATION OF 5.4-CM CIRCULAR CONE AT SPEED OF 5.6 CM/SEC

Reproduced from
best available copy.

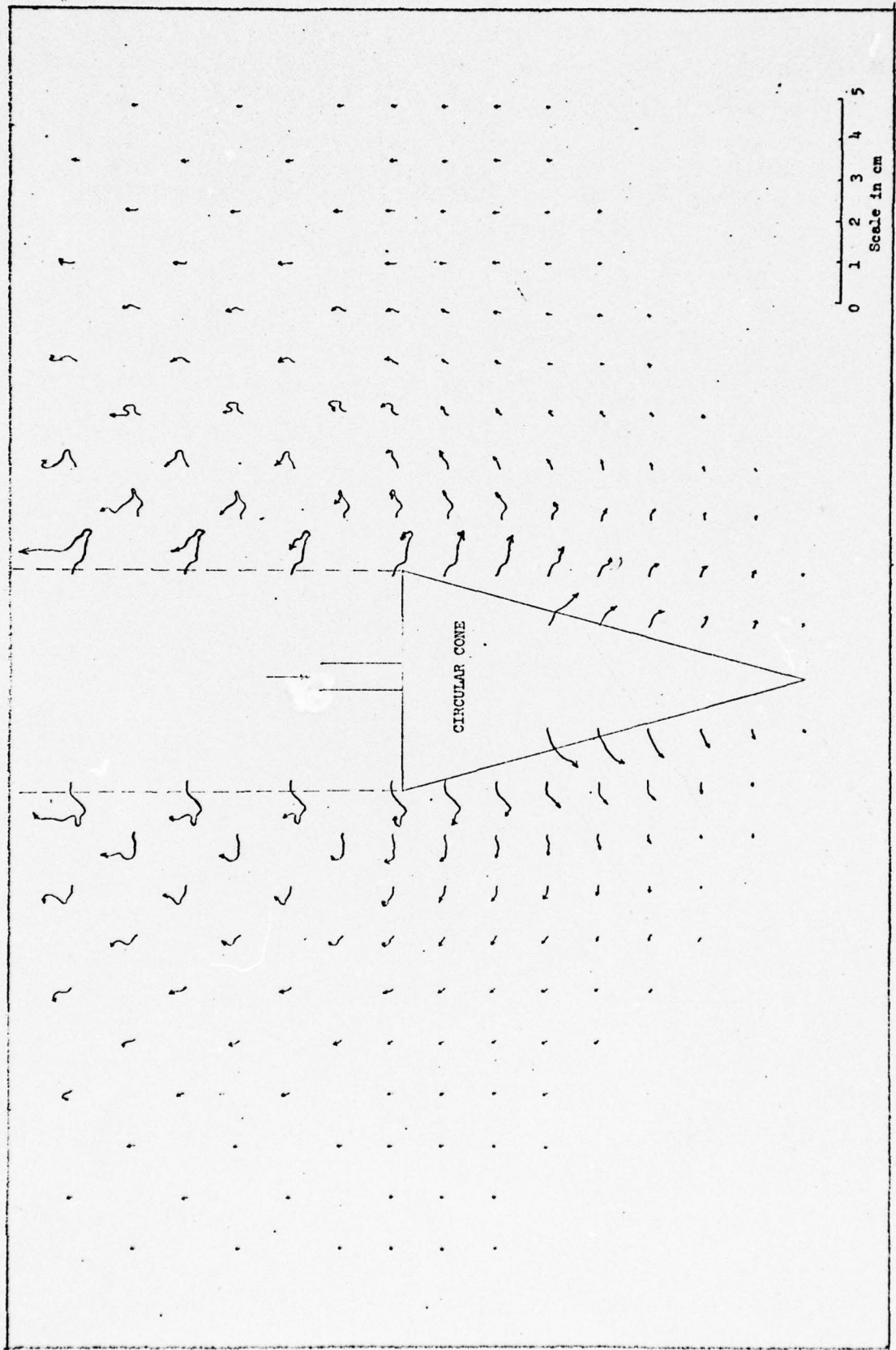
31

PLATE I

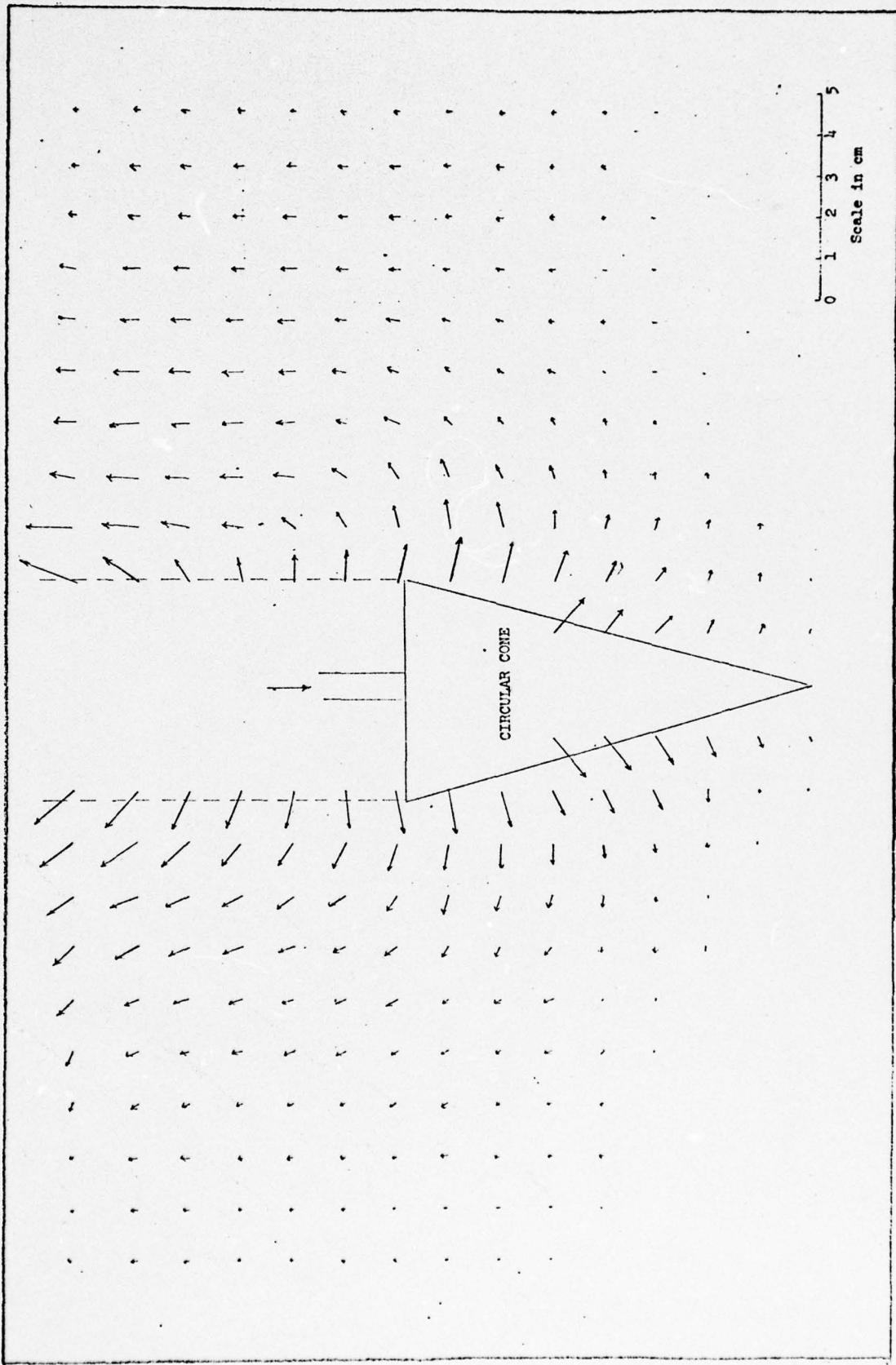


STREAM LINES OF SOIL PARTICLES AROUND A 5.4-CM CIRCULAR CONE; PENETRATION SPEED: 5.6 CM/SEC

32



SOIL PARTICLE MOVEMENT AROUND A 5.4-CM CIRCULAR CONE; PENETRATION SPEED: 5.6 CM/SEC



DISPLACEMENT BENEATH A 5.4-CM CIRCULAR CONE; PENETRATION SPEED: 5.6 CM/SEC

34

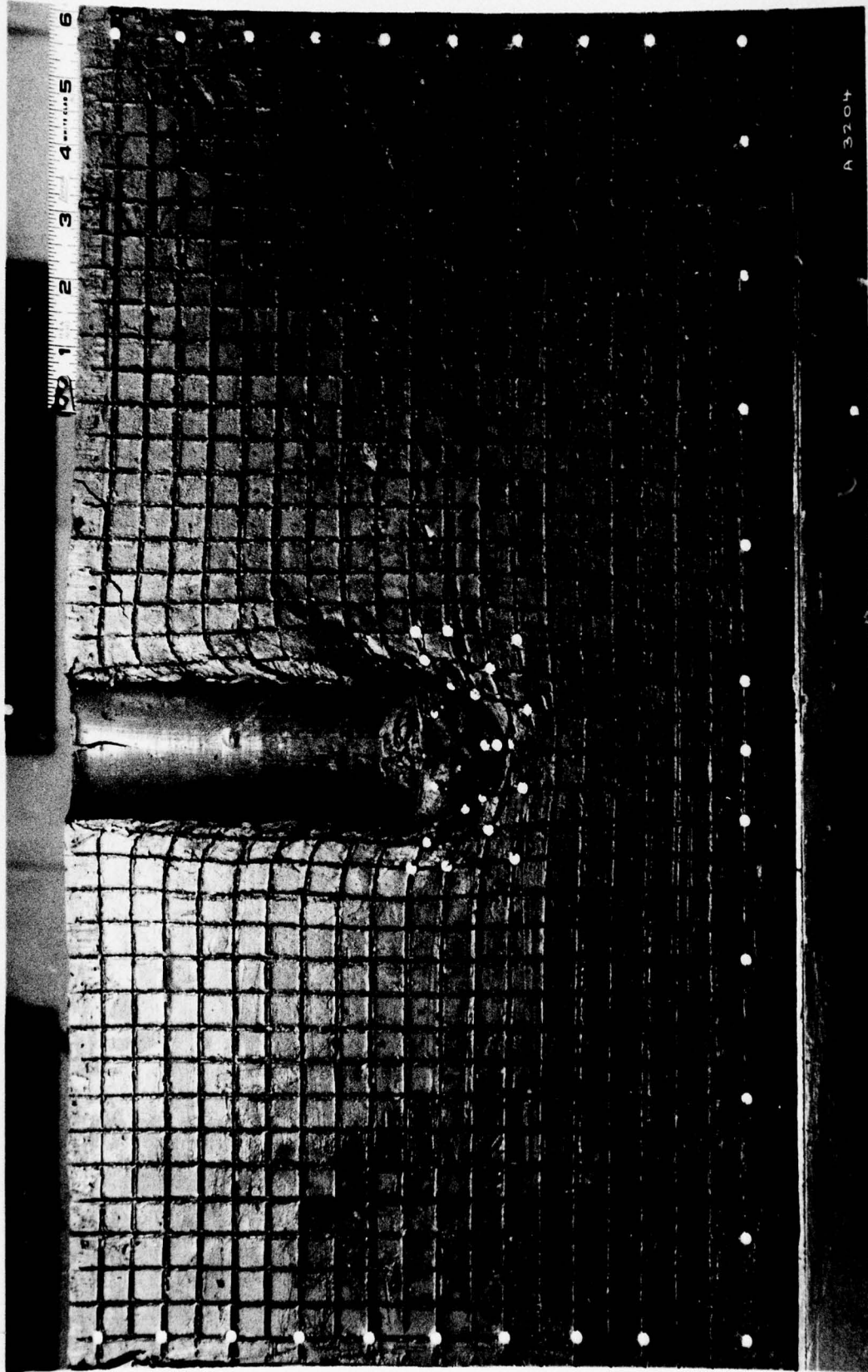


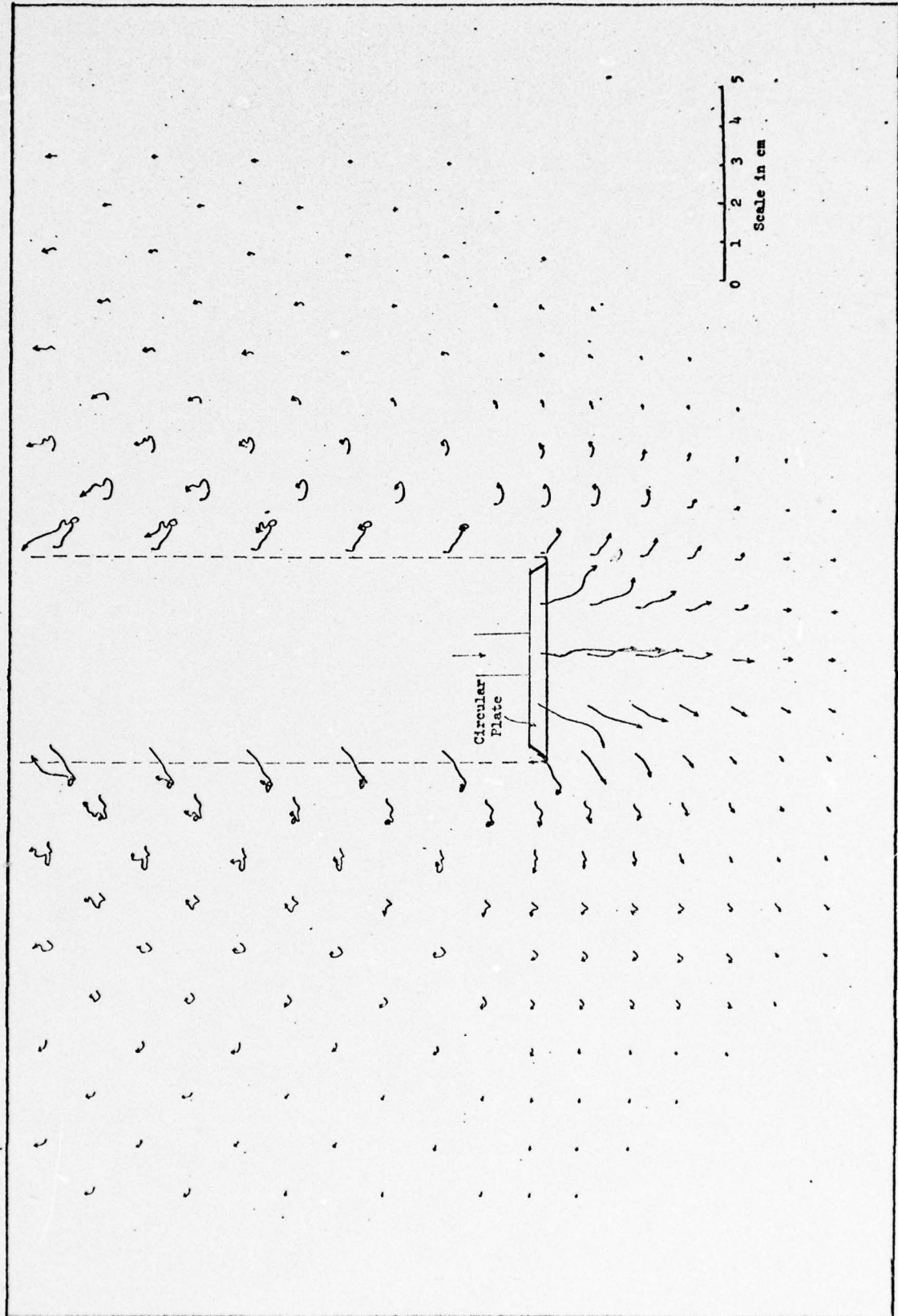
PLATE 5

SOIL FLOW PATTERN AFTER PENETRATION OF 5.1-CM CIRCULAR PLATE AT SPEED OF 0.004 CM/SEC

Reproduced from
best available copy.

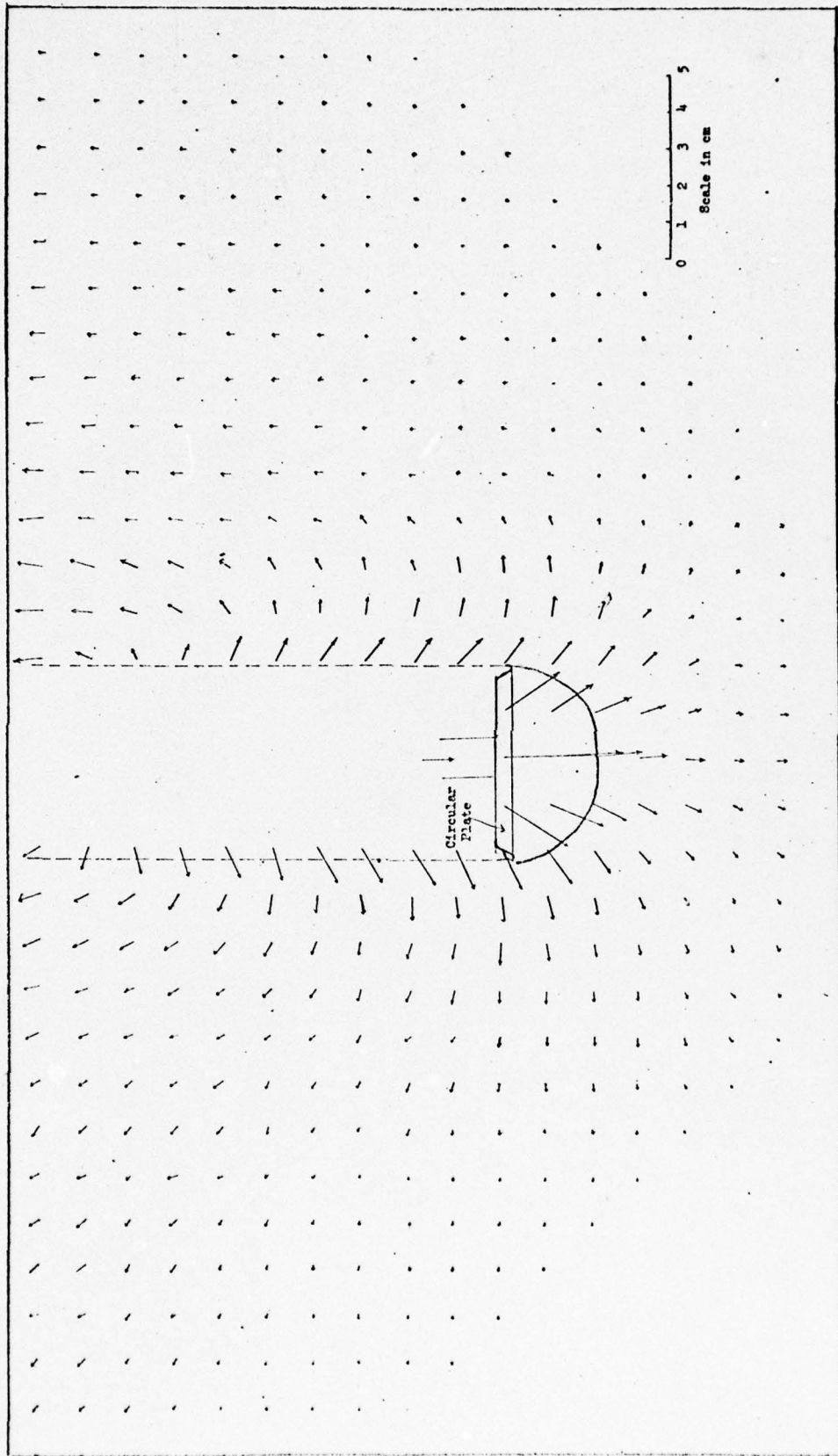
35

A 3204



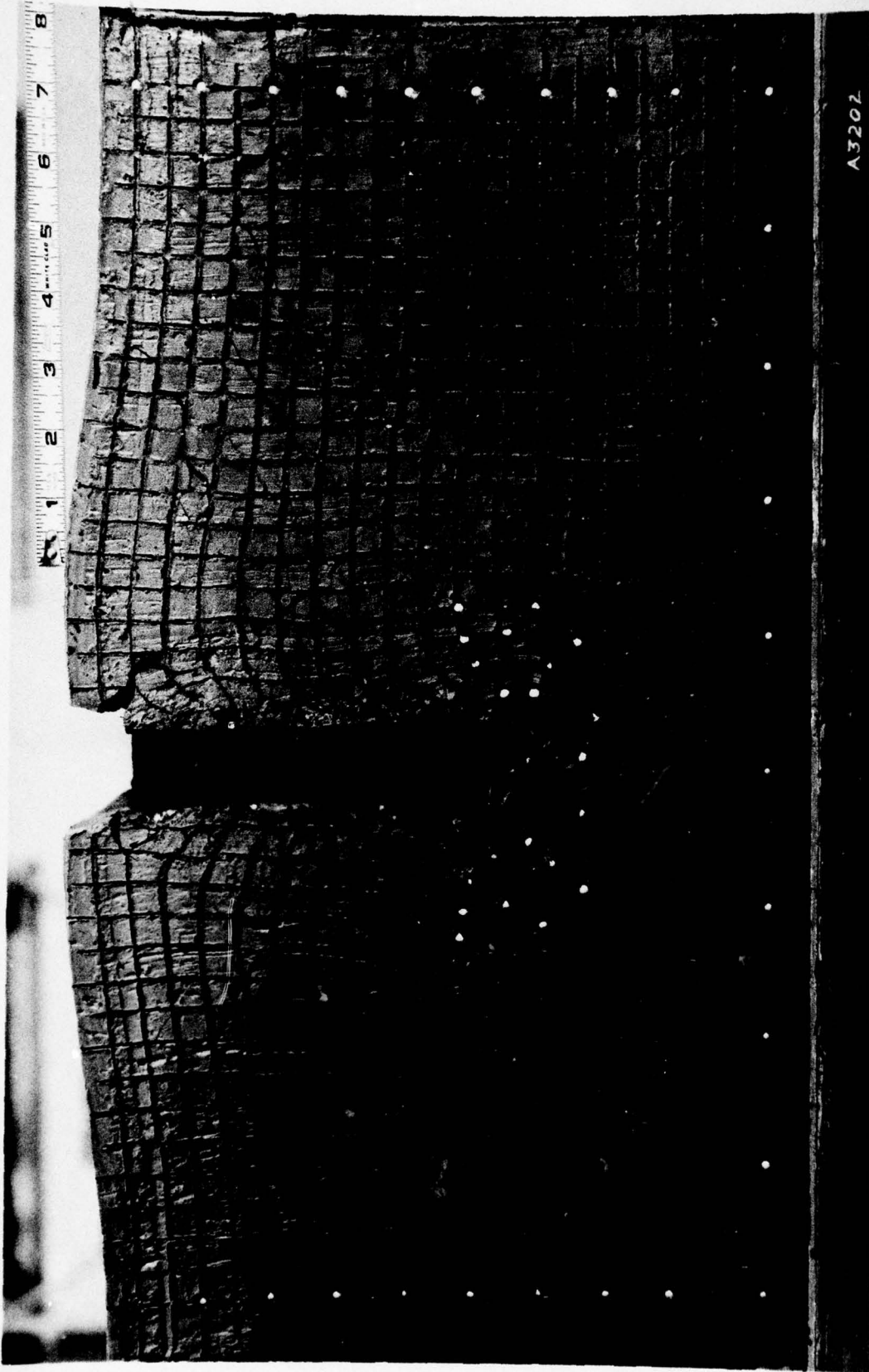
SOIL PARTICLE MOVEMENT AROUND A 5.1-CM CIRCULAR PLATE; PENETRATION SPEED: 0.004 CM/SEC

36



DISPLACEMENT BENEATH A 5.1-CM CIRCULAR PLATE; PENETRATION SPEED: 0.004 CM/SEC

37

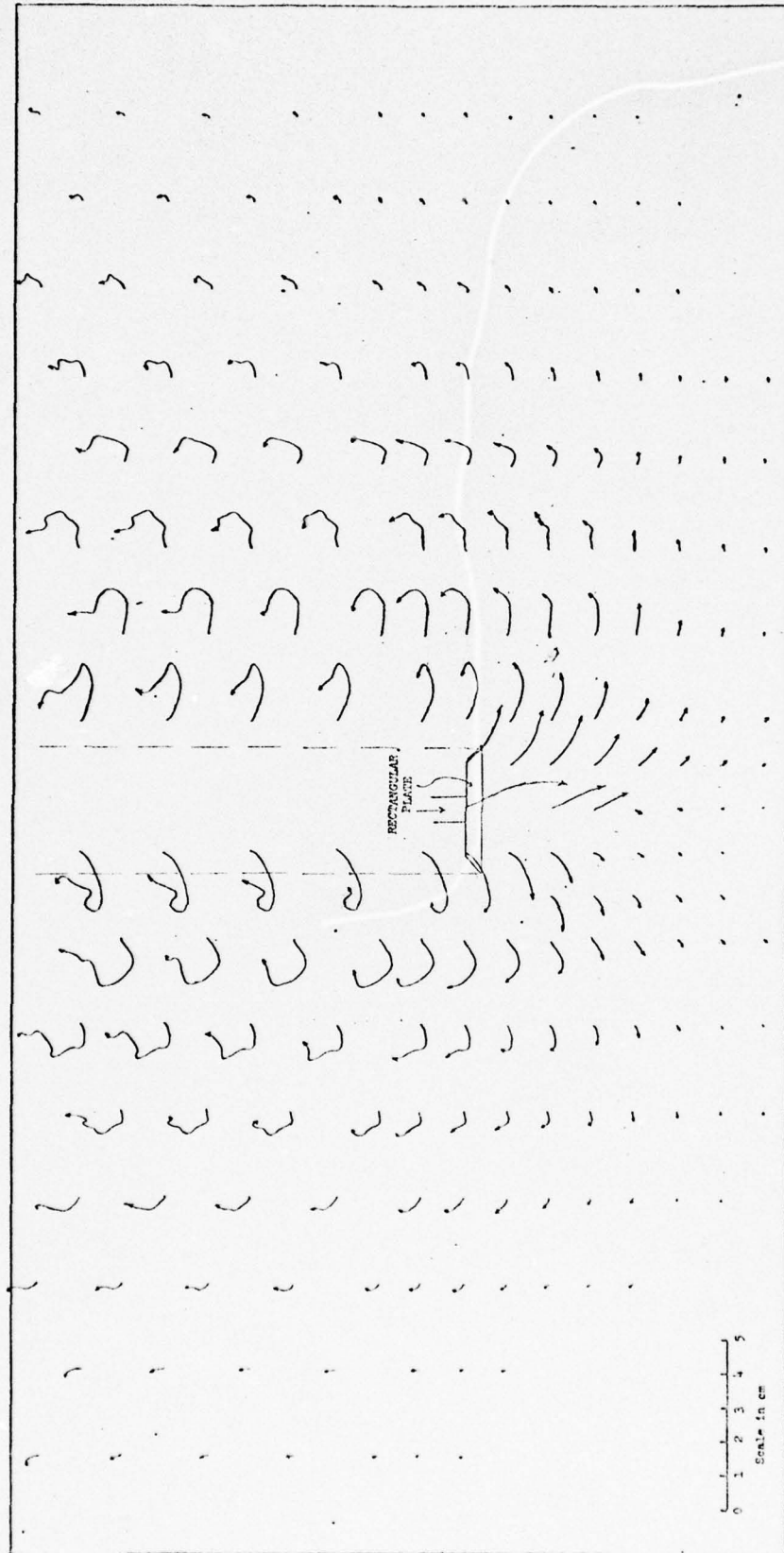


A3207

SOIL FLOW PATTERN AFTER PENETRATION OF 3.8- BY 22.8-CM RECTANGULAR PLATE AT SPEED OF 0.004 CM/SEC

Reproduced from
best available copy.

58



SOIL PARTICLE MOVEMENT AROUND A 3.8- BY 22.8-CM RECTANGULAR PLATE; PENETRATION SPEED: 0.004 CM/SEC

39

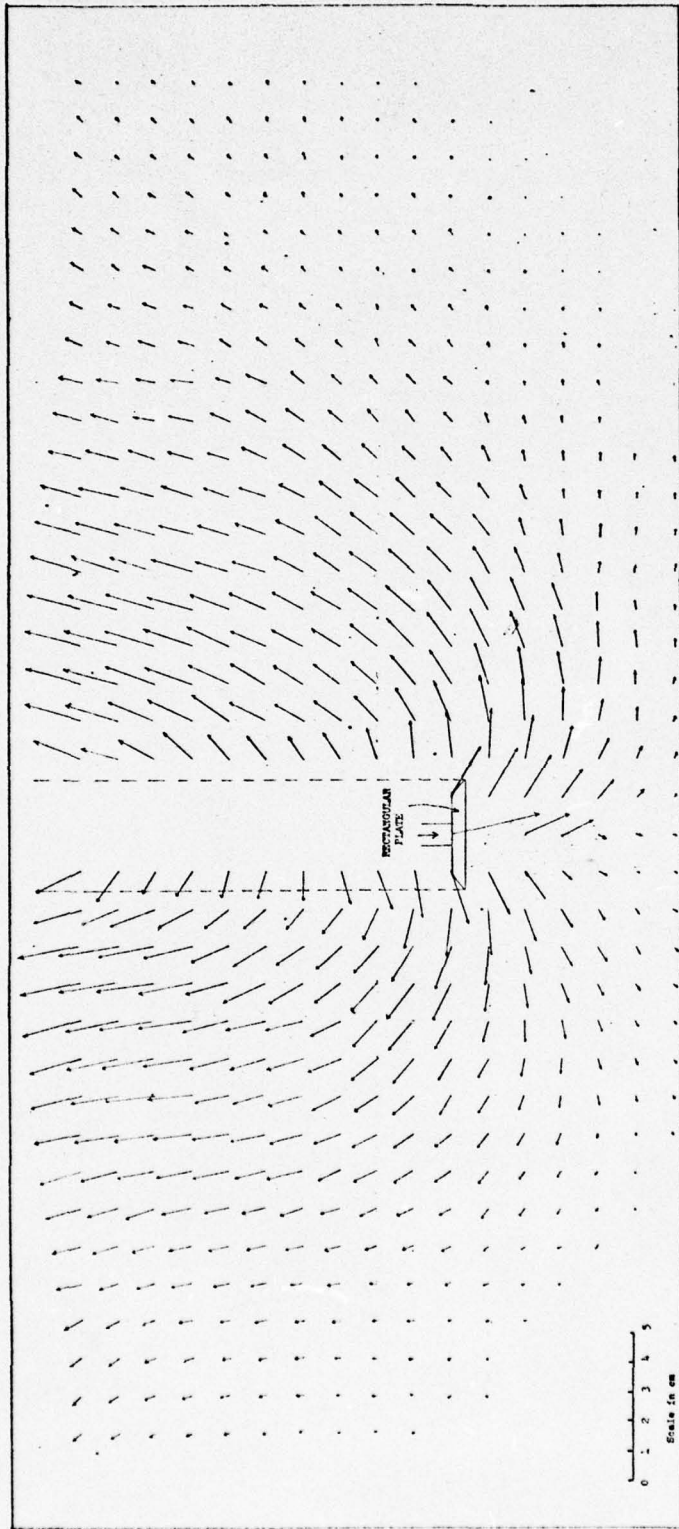
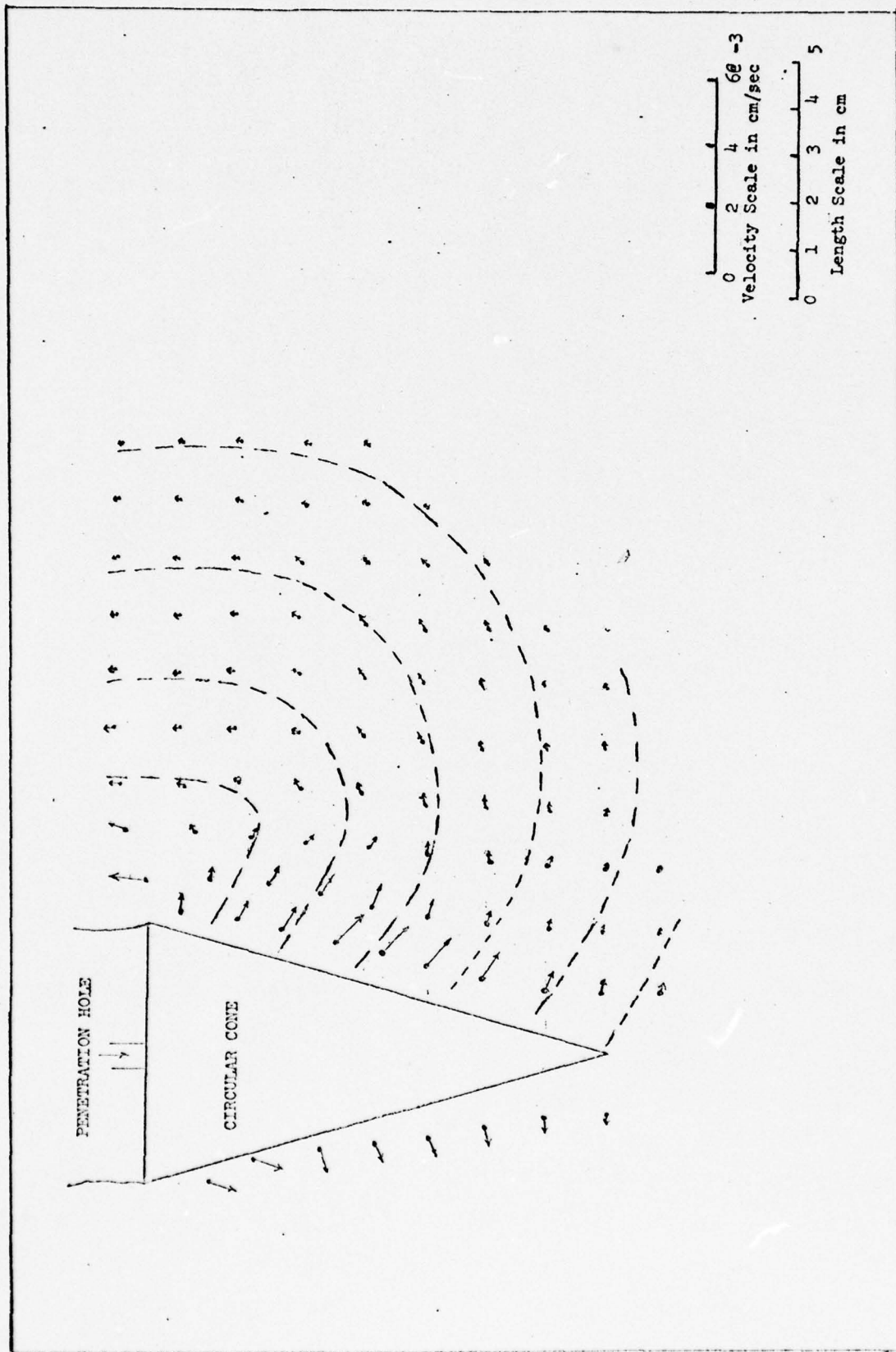


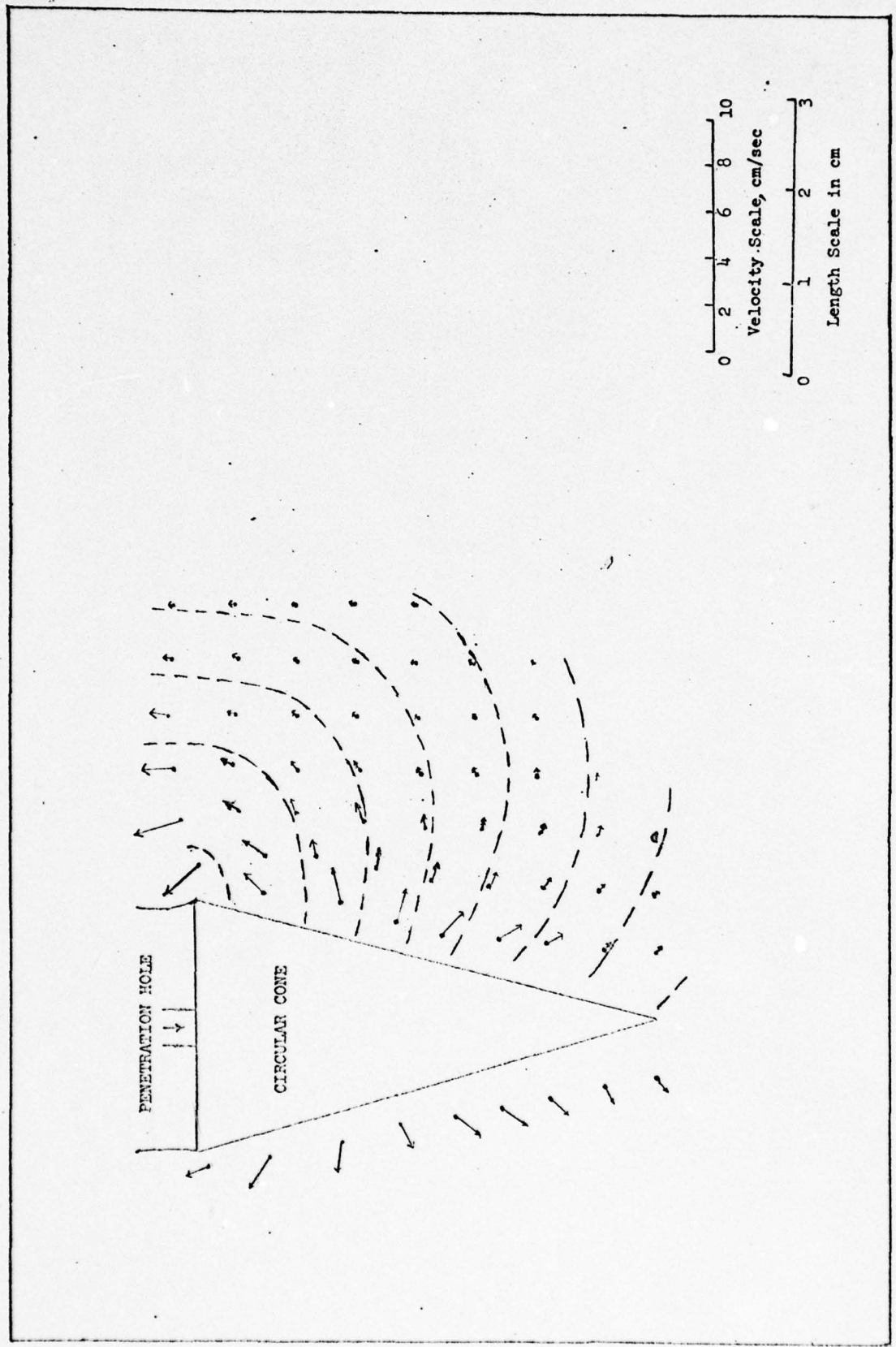
PLATE 10

DISPLACEMENT BENEATH A 3.8- BY 22.8-CM RECTANGULAR PLATE; PENETRATION SPEED: 0.004 CM/SEC

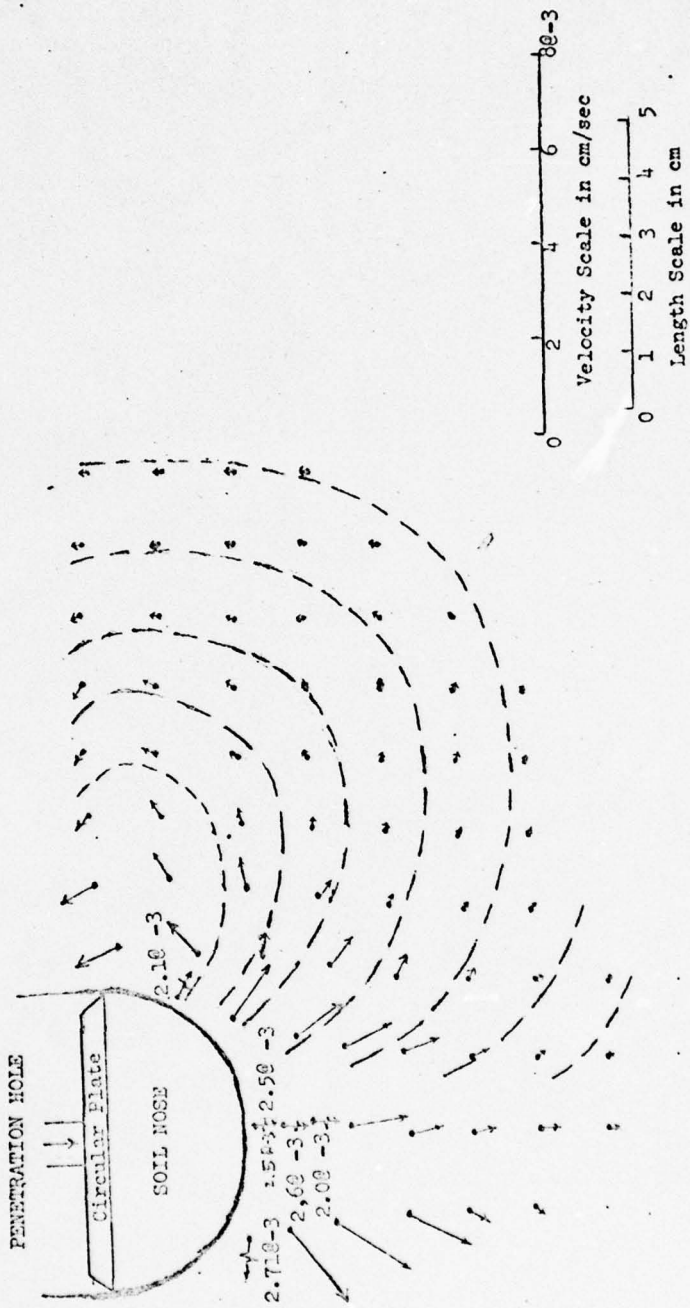


VELOCITY FIELD BENEATH A 5.4-CM CIRCULAR CONE; PENETRATION SPEED: 0.004 CM/SEC

41

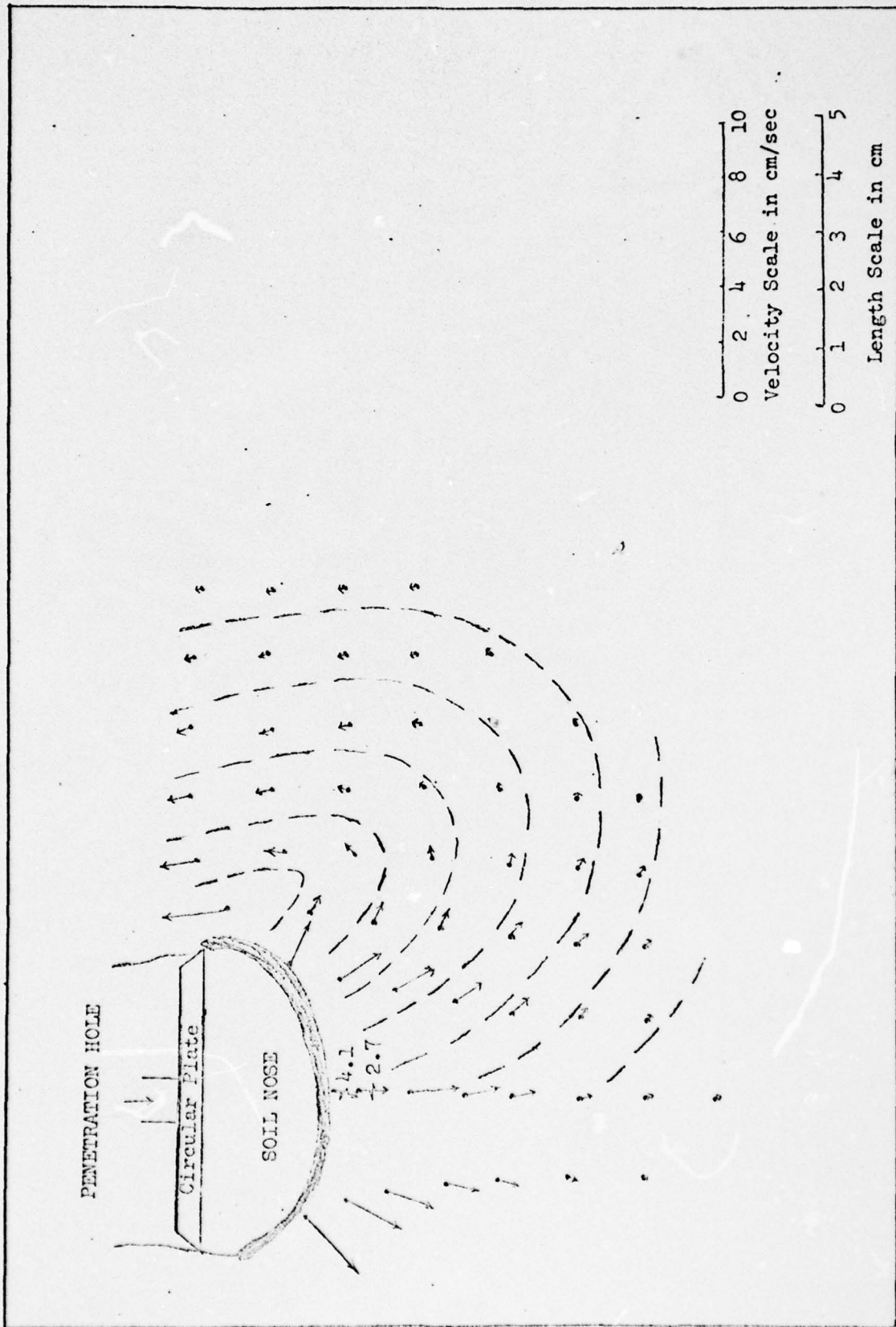


VELOCITY FIELD BENEATH A 5.4-CM CIRCULAR CONE; PENETRATION SPEED: 5.6 CM/SEC
#2



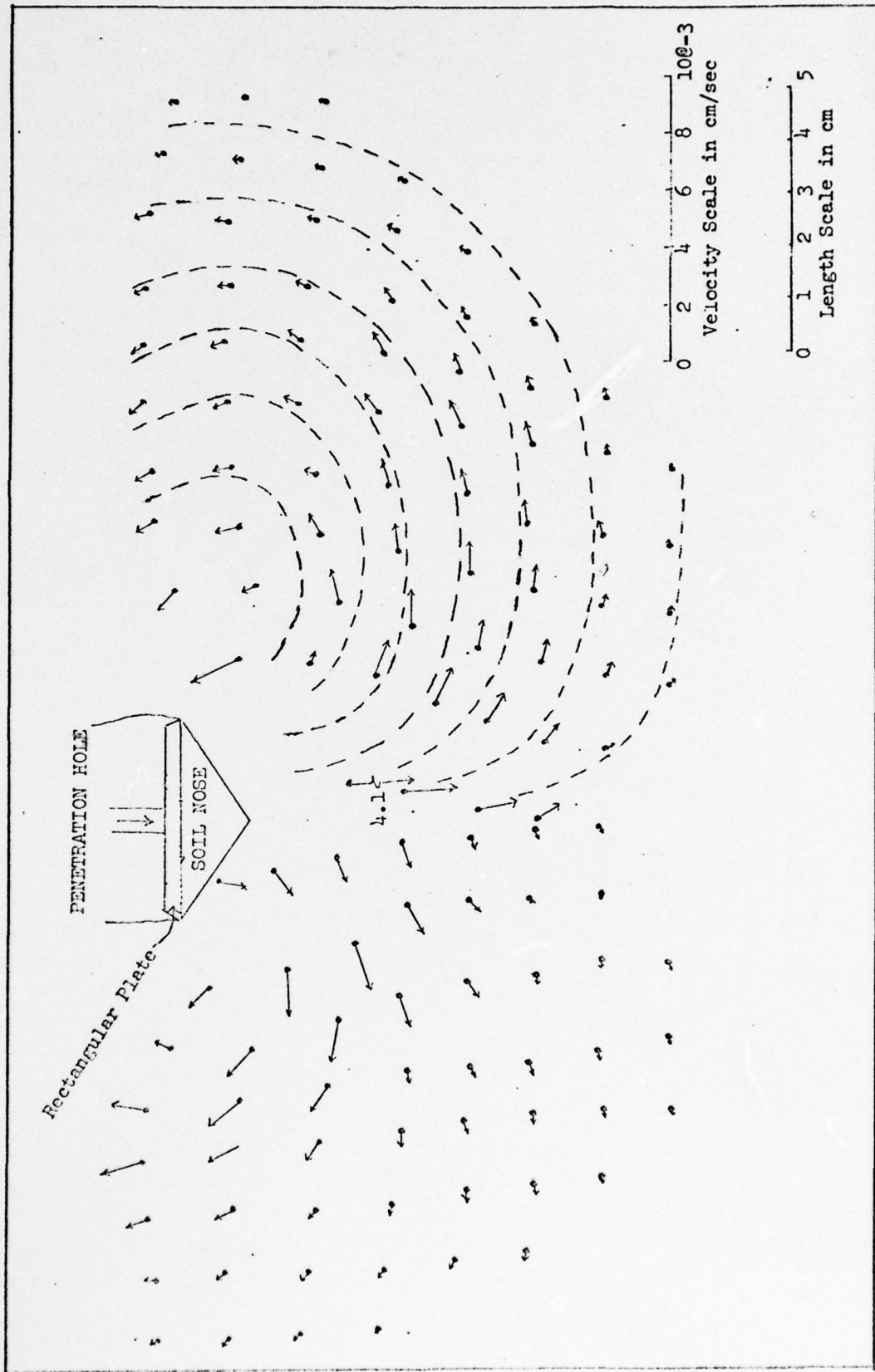
VELOCITY FIELD BENEATH A 5.1-CM CIRCULAR PLATE; PENETRATION SPEED: 0.004 CM/SEC

43



VELOCITY FIELD BENEATH A 5.1-CM CIRCULAR PLATE; PENETRATION SPEED: 5.6 CM/SEC

44



VELOCITY FIELD BENEATH A 3.8- BY 22.9-CM RECTANGULAR PLATE; PENETRATION SPEED: 0.004 CM/SEC

45

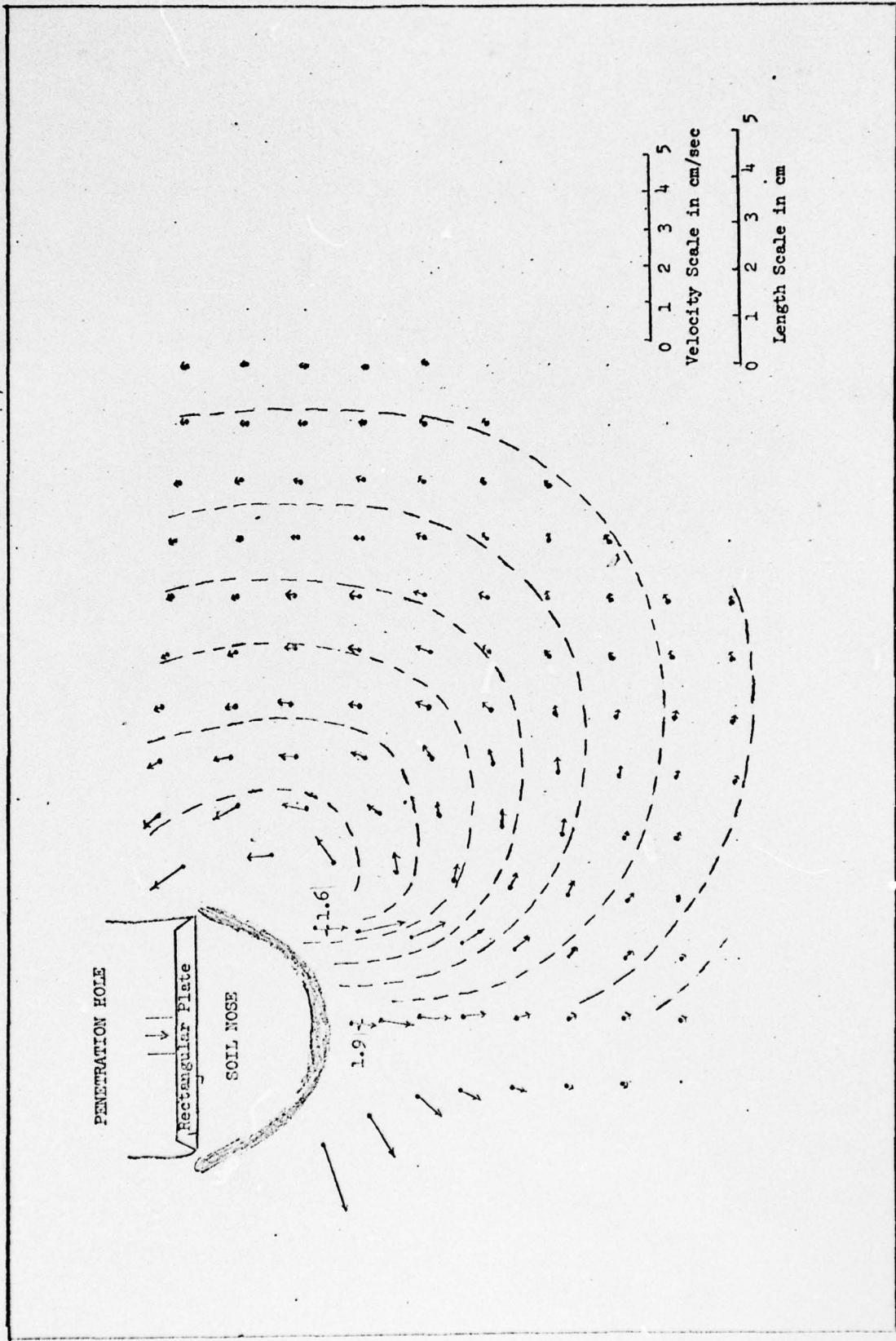


PLATE 16

VELOCITY FIELD BENEATH A 5.1- BY 25.4-CM RECTANGULAR PLATE; PENETRATION SPEED: 3.1 CM/SEC
46

Appendix A: Computer Program

THE GE-400 SERIES - FORTRAN ASA (DAPS)

PAGE # 1 CHOU

```

C      Y.T.CHOU  MOBILITY RESEARCH BRANCH,  W.E.S.
C      PURPOSE:COMPUTATION OF STRAIN RATE FIELD  IN THE SOIL MEDIUM.
1      DIMENSION  R(21),Z(21),A1(9),A2(9),B2(9),A3(9),B3(9),A4(16),
      184(16),  A(9),B(9),VR1(21),VZ1(21),VR2(16,21),VZ2(16,21),VR(16,
      1      21),VZ(16,21),RR(16,21),CEDA(16,21),VEL(16,21),VRR(16,
      121),VRZ(16,21),VZR(16,21),VZZ(16,21),IP3(15),  ZA(15),TB(15),ZB(
      115),RA(15),YA(21),ZC(15),A5(16),B5(16),IP4(15)
2      COMMON  X(21),Y(21),C(16),M,IP,LP,NR,NR1,CHECK
3      EQUIVALENCE (VZ2(16,21),VZ(16,21),VZZ(16,21)), (VR2(16,21),VR(16,
      121)), (RR(16,21),VEL(16,21),CEDA(16,21),VRZ(16,21)), (ZA(15),
      1TB(15),ZB(15),RA(15),ZC(15))
4      READ  9000,  JJ1
5      DO  3000  JJ=1,JJ1
6      PRINT 1020
7      1020 FORMAT (1H1,
      1      40X,48HPURPOSE:COMPUTATIONS OF SOIL STRAIN RATE FIELD  //)
8      READ 1,N11,N12,N2A,N2B,N2C,K1,IP,LP,NR,NR1,RES,V,CONE1,CONE2,
      1      SHEAR1
9      1 FORMAT (10I5,F5.1,F10.8,3F5.1)
10     READ 9000, N2AA,N2BB,NSAVE,NSAVEA,NSAVEE,NO1,NO2,NO3,NO4,NHA,NHB,
      1      NHC,NHD
11     READ  9000,  NH1,NH2,NH3,NH4,NH5,NH6,NUMBER,IP1,IP2
12     9000 FORMAT (16I5 )
13     READ  2001,  DIST1,DIST2,AREA1,AREA2,SQUARE
14     2001 FORMAT (8F10.5)
15     IF (CONE1-1) 1001,1002,1003
16     1001 IF (CONE2-1) 1004,1005,1005
17     1004 PRINT 1010
18     1010 FORMAT (20X,40HPROJECTOR:2 IN BY 10 IN SQUARE PLATE )
19     GO TO 1014
20     1005 PRINT 1011
21     1011 FORMAT (20X,45HPROJECTOR:1.5 IN BY 9 IN SQUARE PLATE )
22     GO TO 1014
23     1002 PRINT 1012
24     1012 FORMAT (20X,45HPROJECTOR:2 IN CIRCULAR PLATE )
25     GO TO 1014
26     1003 PRINT 1013
27     1013 FORMAT (20X,45HPROJECTOR:2 IN CIRCULAR CONE )
28     1014 CONTINUE
29     PRINT 1015 , V,NUMBER
30     1015 FORMAT (20X,29HPENETRATION SPEED(INCH/SEC.)=F10.8,10X,15HTEST
      1NUMBER=I5 )
31     TINC=SQUARE/V
32     SUM=0.
33     DO  1000  J=1,2
34     DO 81  M1=1,16
35     DO 82  M2=1,21
36     VR2(M1,M2)=0.
37     VZ2(M1,M2)=0.
38     RR(M1,M2)=0.
39     82 CONTINUE
40     81 CONTINUE
41     DO  296  M3=1,21
42     VR1(M3)=0.

```

```

43      VZ1(M3)=0.
44      296 CONTINUE
45      IF (J-1) 1030,1030,1031
46      1030 N1=N11
47          NSAVEB=ND1
48      PRINT 212
49      212 FORMAT (/9X,40H THE COMPUTED RESULTS ON THE RIGHT SIDE )
50      GO TO 1032
51      1031 N1=N12
52          NSAVEB=N02
53      PRINT 214
54      214 FORMAT (/9X,40H THE COMPUTED RESULTS ON THE LEFT SIDE
55      1032 CONTINUE
56      READ 9000, (IP3(I),I=NSAVE,NSAVEE)
57      READ 9000, (IP4(I),I=1,N1)
58      DO 2 I1=1,N1
59      IF (I1-2) 100,100,101
60      100 IF (I1-1) 102,102,103
61      102 N2=N2A
62          N22=N2AA
63      GO TO 104
64      103 N2=N2B
65          N22=N2BB
66      GO TO 104
67      101 N2=N2C
68          N22=N2C
69      104 READ 1044, (R(I),I=1,N2)
70      READ 1044, (Z(I),I=1,N2)
71      1044 FORMAT (16F5.2)
72      PRINT 5044, I1
73      5044 FORMAT (/24H THE VALUES OF R AND Z IN I2,11TH COLUMN )
74      PRINT 1044, (R(I),I=1,N2)
75      PRINT 1044, (Z(I),I=1,N2)
76      M=N2
77      IF (I1-3) 9950,9951,9950
78      9951 IP=IP1
79          LP=IP
80      GO TO 9954
81      9950 IF (I1-4) 9952,9953,9952
82      9953 IP=IP1
83          LP=IP
84      GO TO 9954
85      9952 IP=IP2
86          LP=IP
87      9954 CONTINUE
88      DO 4 I=1,N2
89      X(I)=Z(I)
90      Y(I)=R(I)
91      4 CONTINUE
92      IF (I1-5) 9500,9500,9501
93      9500 CHECK=NHC
94      9501 CONTINUE
95      CALL LEAST
96      LPP=LP+1

```

```

97      DO      5      I=1,LPP
98      5 A1(I)=C(I)
99      IF (I1-5)      1035,1035,1036
100     1035 PRINT 1037, (A1(I),I=1,LPP)
101     1037 FORMAT      (10E12.5)
102     1036 CONTINUE
103     IF (J-1)      7006,7006,7002
104     7006 IF (NH1)      7002,7002,7001
105     7001 IF (I1-5)      7000,7000,7002
106     7000 PRINT 7005
107     7005 FORMAT (/35H CHECK STATION NUMBER ONE :1
108           ZZ=-0.5
109           DO      7003      I=1,15
110           ZA(I)=ZZ+0.5
111           RZ =A1(1)+A1(2)*ZA(I)+A1(3)*ZA(I)**2
112           IF (LP-2)      60,60,61
113           61 DO      62      I2=3,LP
114           IS =I2+1
115           TE1=A1(IS )*ZA(I)**I2
116           RZ=RZ+TE1
117           62 CONTINUE
118           60 CONTINUE
119           PRINT 7004, ZA(I),RZ
120           7004 FORMAT (2HZ=F5.2,40X,2HR=F10.5 )
121           ZZ=ZA(I)
122           7003 CONTINUE
123           7002 CONTINUE
124           DO      6      I=2,N2
125           SUB=I-1
126           X(I)=SUB*11NC
127           Y(I)=R(I)-R(1)
128           YA(I)=Y(I)
129           X(1)=0.
130           Y(1)=0.
131           6 CONTINUE
132           CALL LEAST
133           LPP=LP+1
134           DO      7      I=1,LPP
135           7 A2(I)=C(I)
136           Y(1)=0.
137           R(1)=0.
138           DO      8      I=2,N2
139           SUB=I-1
140           Y(I)=SUB*0.5-7(I)
141           8 CONTINUE
142           CHECK=NHC
143           CALL LEAST
144           LPP=LP+1
145           DO      9      I=1,LPP
146           9 B2(I)=C(I)
147           IF (J-1)      7015,7015,7010
148           7015 IF (NH2)      7010,7010,7011
149           7011 IF (I1-3)      7010,7012,7010
150           7012 PRINT 7019

```

```
7019 FORMAT (// 45H CHECK STATION NUMBER TWO :2 (U,W ) )
PRINT 9980, (X(I), I=1,N2)
PRINT 9980, (YA(I),I=1,N2)
PRINT 9980, (Y(I),I=1,N2)
9980 FORMAT (12E10.3)
TT=-TINC/2.
DO 7013 I=1,16
TB(I)=TT +TINC/2.
WA=B2(1)+B2(2)*TB(I)+B2(3)*TB(I)**2
IF (LP-2) 70,70,71
71 DO 72 I2=3,LP
IRR =I2+1
TE1=B2(IRR)*TB(I)**I2
WA=WA+TE1
72 CONTINUE
70 CONTINUE
PRINT 7014, TB(I),WA
7014 FORMAT (2HT=F5.2,40X,2HW=F10.4 )
TT =TB(I)
7013 CONTINUE
7010 CONTINUE
IF (NHA) 291,291,292
292 PRINT 293, J,I1
293 FORMAT (//60X,16HBRAIN WASH AT J=12.5X, 6HCOLUMN 13, 8HU THEN W/)
PRINT 9980, (X(I), I=1,N2)
PRINT 9980, (YA(I),I=1,N2)
PRINT 9980, (Y(I),I=1,N2)
291 CONTINUE
DO 10 I=2,N2
SUB=I-1
VR1(I)=A2(2)+2.*A2(3)*TINC*SUB
VZ1(I)=B2(2)+2.*B2(3)*TINC*SUB
IF (LP-2) 50,50,51
51 DO 53 I2=3,LP
IQ1=I2-1
IQ2=I2+1
T=I2
TE1=T*A2(IQ2)*(TINC*SUB)**IQ1
TE2=T*B2(IQ2)*(TINC*SUB)**IQ1
VR1(I)=VR1(I)+TE1
VZ1(I)=VZ1(I)+TE2
53 CONTINUE
50 CONTINUE
10 CONTINUE
VR1(1)=0.
VZ1(1)=0.
DO 11 I=1,N2
X(I)=Z(I)
Y(I)=VR1(I)
YA(I)=Y(I)
11 CONTINUE
IF (I1-1) 9502,9502,9503
9502 CHECK=NHC
9503 CONTINUE
```

```

205      M=N2
206      CALL LEAST
207      LPP=LP+1
208      DO      12      I=1,LPP
209      12  A3(I)=C(I)
210      IF (I1-1) 6000,6000,6001
211      6000 PRINT 1037, (A3(I),I=1,LPP)
212      6001 CONTINUE
213      DO      13      I=1,N2
214      13  Y(I)=VZ1(I)
215      CALL LEAST
216      LPP=LP+1
217      DO      14      I=1,LPP
218      14  B3(I)=C(I)
219      IF (J-1) 7025,7025,7020
220      7025 IF (NH3) 7020,7020,7021
221      7021 IF (I1-3) 7020,7022,7020
222      7022 PRINT 7029
223      7029 FORMAT (// 40H CHECK STATION NUMBER,THREE:3 (VR VZ )
224      PRINT 9980, (X(I), I=1,N2)
225      PRINT 9980, (YA(I),I=1,N2)
226      PRINT 9980, (Y(I),I=1,N2)
227      ZZ=-1.
228      DO      7023      I=1,10
229      ZB(I)=ZZ+1.
230      VV=B3(1)+B3(2)*ZB(I)+B3(3)*ZB(I)**2
231      IF (LP-2) 86,86,87
232      87  DO 88      I2=3,LP
233      IQ1=I2+1
234      TE1=B3(IQ1)*ZB(I)**I2
235      VV=VV+TE1
236      88 CONTINUE
237      86 CONTINUE
238      PRINT 7024, ZB(I),VV
239      7024 FORMAT (2HZ=F5.2,40X,24HVELOCITY IN Z DIRECTION=F14.8 )
240      ZZ=ZB(I)
241      7023 CONTINUE
242      7020 CONTINUE
243      IF (NH8) 294,294,7085
244      7085 PRINT 7086, J,I1
245      7086 FORMAT (//60X,16HBRAIN WASH AT J=I2,5X, 6HCOLUMN I3,9HVR AND VZ/)
246      PRINT 9980, (X(I), I=1,N2)
247      PRINT 9980, (YA(I),I=1,N2)
248      PRINT 9980, (Y(I),I=1,N2)
249      294 CONTINUE
250      DO      15      I2=NSAVE,N22
251      SUB=I2-1
252      VR2(I1,I2)=A3(1)+A3(2)*SUB*0.5+A3(3)*((SUB*0.5)**2)
253      VZ2(I1,I2)=B3(1)+B3(2)*SUB*0.5+B3(3)*((SUB*0.5)**2)
254      RR(I1,I2)=A1(1)+A1(2)*SUB*0.5+A1(3)*((SUB*0.5)**2)
255      IF (LP-2) 90,90,91
256      91  DO 92      I=3,LP
257      IQ1=I+1
258      TE1=A3(IQ1)*((SUB*0.5)**I)

```

```

259      TE2=B3( IQ1)*(SUB*0.5)**I
260      TE3=A1(IQ1)*(SUB*0.5)**I
261      VR2(I1,I2)=VR2(I1,I2)+TE1
262      VZ2(I1,I2)=VZ2(I1,I2)+TE2
263      RR(I1,I2)=RR(I1,I2)+TE3
264      92 CONTINUE
265      90 CONTINUE
266      IF (RR(1,I2)-0.0000001) 301,301,302
267      301 RR(1,I2)=0.
268      302 CONTINUE
269      15 CONTINUE
270      DO 4000 I=1,N22
271      VR2(1,I)=VR2(2,I)
272      VZ2(1,I)=VZ2(2,I)
273      4000 CONTINUE
274      IF (J-1) 7036,7036,7030
275      7036 IF (NH4) 7030,7030,7031
276      7031 IF (I1-3) 7032,7032,7030
277      7032 PRINT 7039, I1
278      7039 FORMAT (// 52H CHECK STATION NUMBER FOUR:4 THE RR DISTANCE IN
1          I5,20HTH COLUMN )
279      PRINT 7035, (RR(I1,I2),I2=NSAVE,N22)
280      PRINT 7035, (VR2(I1,I2),I2=NSAVE,N22)
281      PRINT 7035, (VZ2(I1,I2),I2=NSAVE,N22)
282      7035 FORMAT (12E10.3)
283      7030 CONTINUE
284      2 CONTINUE
285      PRINT 7073
286      7073 FORMAT (40X,30H LOOP 2 PRINT OUT COMPLETED )
287      N2=NSAVEE
288      DO 20 I2=NSAVE,N2
289      IP=IP3(I2)
290      LP=IP
291      IF (I2-N2AA) 200,200,201
292      200 NA=1
293      GO TO 202
294      201 IF (I2-N2BB) 203,203,204
295      203 NA=2
296      GO TO 202
297      204 NA=3
298      202 CONTINUE
299      M=N1-NA+1
300      DO 21 I1=NA,N1
301      I=I1-(NA-1)
302      X(I)=RR(I1,I2)
303      Y(I)=VR2(I1,I2)
304      YA(I)=Y(I)
305      21 CONTINUE
306      IF (I2-N2AA) 9505,9505,9504
307      9505 CHECK=NHC
308      9504 CONTINUE
309      CALL LEAST
310      LPP=LP+1
311      DO 22 I=1,LPP

```

```

312      22 A4(I)=C(I).
313      IF (I2-N2AA) 6010,6011,6010
314      6011 PRINT 1037, (A4(I),I=1,LPP)
315      6010 CONTINUE
316      DO 23
317      I=I1-(NA-1)
318      23 Y(I)=VZ2(I1,I2)
319      CHECK=NHC
320      CALL LEAST
321      LPP=LP+1
322      DO 24
323      24 B4(I)=C(I)
324      IF (J-1) 7043,7043,7040
325      /043 IF (NH5) 7040,7040,7041
326      7041 IF (I2-N2AA) 305,305, 7040
327      305 PRINT /045,IP
328      7045 FORMAT (//21HCHECK STATION NO.5:
329      PRINT /046, I2
330      7046 FORMAT (50H VELOCITY IN Z DIRECTION ALONG HORIZONTAL LINE. I2=I2 )
331      PRINT 7047., (VZ2(I1,I2), I1=1,N1 )
332      /047 FORMAT (12E10.3)
333      PRINT /048
334      7048 FORMAT (50H THE CORRESPONDING RR, THEN CORREPPONDING VR AND VZ )
335      PRINT /047 , (RR(I1,I2), I1=1,N1 )
336      PRINT 9980, (X(I), I=1,N1)
337      PRINT 9980, (YA(I),I=1,N1)
338      PRINT 9980, (Y(I),I=1,N1)
339      RAA=-0.25
340      DO 7050
341      RA(I)=RAA+0.25
342      VRA=A4(1)+A4(2)*RA(I)+A4(3)*RA(I)**2
343      VZA=B4(1)+B4(2)*RA(I)+B4(3)*RA(I)**2
344      IF (LP-2) 95,95,96
345      96 DO 97
346      IQ1=I1+1
347      TE1=A4(IQ1)*RA(I)**I1
348      TE2=B4(IQ1)*RA(I)**I1
349      VRA=VRA+TE1
350      VZA=VZA+TE2
351      97 CONTINUE
352      95 CONTINUE
353      PRINT /051, RA(I),VRA,VZA
354      7051 FORMAT (2HR=F5.2,20X,4HVR= E12.5,20X,4HVZ= E12.5)
355      RAA=RA(I)
356      7050 CONTINUE
357      7040 CONTINUE
358      DO 25
359      SUB=I1-1
360      VR(I1,I2)=A4(1)+A4(2)*SUB*0.5+A4(3)*(SUB*0.5)**2
361      VZ(I1,I2)=B4(1)+B4(2)*SUB*0.5+B4(3)*(SUB*0.5)**2
362      IF (LP-2) 120,120,121
363      121 DO 122
364      IQ1= I+1
365      TE1=A4(IQ1)*(SUB*0.5)**I

```

```

366      TE2=B4(IQ1)*(SUB*0.5)**I
367      VR(I1,I2)=VR(I1,I2)+TE1
368      VZ(I1,I2)=VZ(I1,I2)+TE2
369      122 CONTINUE
370      120 CONTINUE
371      VEL(I1,I2)=SQRT(VR(I1,I2)**2+VZ(I1,I2)**2)
372      25 CONTINUE
373      PRINT 26, I2
374      26 FORMAT (/ 48H THE COMPUTED VELOCITIES AT GRID POINTS ALONG
113,44H THE ROW(COUNTED FROM THE BOTTOM OF THE MOLD) )
375      PRINT 9002, (VEL(I1,I2),I1=1,N1)
376      9002 FORMAT (12E10.3)
377      PRINT 9998
378      9998 FORMAT (10X,5HVZ: )
379      PRINT 9002, (VZ(I,I2),I=1,N1 )
380      PRINT 9997
381      9997 FORMAT (10X,5HVR: )
382      PRINT 9002, (VR(I,I2),I=1,N1 )
383      DO 27 I1=NA,N1
384      27 CEDA(I1,I2)=ATAN(VZ(I1,I2)/VR(I1,I2))*57.2
385      PRINT 28
386      28 FORMAT (43H THE DEGREE OF ANGLE AT SAME ROW )
387      PRINT 29, (CEDA(I1,I2),I1=1,N1)
388      29 FORMAT (16F7.1)
389      DO 30 I1=NA,N1
390      SUB=I1-1
391      VRR(I1,I2)=A4(2)+2.*A4(3)*SUB*0.5
392      VZR(I1,I2)=B4(2)+2.*B4(3)*SUB*0.5
393      IF (LP-2) 110,110,111
394      111 DO 112 I=3,LP
395      IQ1=I+1
396      IQ2=I-1
397      T=I
398      TE1=T*A4(IQ1)*(SUB*0.5)**IQ2
399      TE2=T*B4(IQ1)*(SUB*0.5)**IQ2
400      VRR(I1,I2)=VRR(I1,I2)+TE1
401      VZR(I1,I2)=VZR(I1,I2)+TE2
402      112 CONTINUE
403      110 CONTINUE
404      30 CONTINUE
405      221 PRINT 222, I2
406      222 FORMAT (40H THE VALUES OF VRR AT GRID POINTS ALONG 13,6H THE ROW )
407      PRINT 223, (VRR(I1,I2),I1=1,N1)
408      223 FORMAT (12E10.3)
409      PRINT 224
410      224 FORMAT (20H )
411      PRINT 223, (VZR(I1,I2),I1=1,N1)
412      220 CONTINUE
C
C
413      20 CONTINUE
C
414      PRINT /071
415      7071 FORMAT (///10X,10H LOOP 20 OK ///)

```

```

416      DO      32      I1=1,N1
417          IP=IP4(I1)
418          LP=IP
419      IF      (I1-2) 230,230,231
420 230 IF      (I1-1) 232,232,233
421 232 N2=N2AA-ND3
422      GO TO 234
423 233 N2=N2BB-ND4
424      GO TO 234
425 231 N2=N2C
426 234 M=N2-NSAVE+1
427      DO      33      I2=NSAVE,N2
428          SUB=I2-1
429          I6=I2-(NSAVE-1)
430          X(I6)=SUB*0.5
431          Y(I6)=VR(I1,I2)
432      33 CONTINUE
433      IF      (I1-3) 9507,9507,9506
434 9507 CHECK=NHC
435 9506 CONTINUE
436      CALL LEAST
437          LPP=LP+1
438      DO      34      I=1,LPP
439      34 A5(I)=C(I)
440      IF      (I1-3) 6020,6021,6021
441 6021 PRINT 1037, (A5(I), I=1,LPP)
442 6020 CONTINUE
443      DO      35      I2=NSAVE,N2
444          I6=I2-(NSAVE-1)
445          Y(I6)=VZ(I1,I2)
446      35 CONTINUE
447      CALL LEAST
448          LPP=LP+1
449      DO      36      I=1,LPP
450      36 B5(I)=C(I)
451          IF      (I1-NSAVE) 3011,3011,7060
452 3011 IF      (J-1) 7063,7063,7060
453 7063 IF      (NH6) 7060,7060,7061
454 7061 PRINT 7064,I1,IP
455 7064 FORMAT (50H VR AND VZ ALONG COLUMN
1 PRINT 7062 , (VR(I1,I2), I2=1,N2C )
PRINT 7062 , (VZ(I1,I2), I2=1,N2C )
7062 FORMAT (10E10.3 )
ZZ=-0.75
460      DO      3006      I=1,I2
461      ZC(I)=ZZ+0.75
462      RZ1=A5(I)+A5(2)*ZC(I)+A5(3)*ZC(I)**2
463      RZ2=B5(I)+B5(2)*ZC(I)+B5(3)*ZC(I)**2
464      IF      (LP-2) 3007,3007,3008
465 3008 DO      3009      I2=3,LP
466          IS=I2+1
467          TE1=A5(IS) *ZC(I)**I2
468          TE2=B5(IS) *ZC(I)**I2

```

```

469      RZ1=RZ1+TE1
470      RZ2=RZ2+TE2
471      3009 CONTINUE
472      3007 CONTINUE
473      PRINT      3010,  ZC(1),RZ1,RZ2
474      3010 FORMAT (E12.5,10X,E12.5,10X,E12.5)
475      ZZ=ZC(1)
476      3006 CONTINUE
477      7060 CONTINUE
478      DO      37      I2=NSAVE,N2
479      SUB=I2-1
480      VRZ(11,I2)=A5(2)+2.*A5(3)*SUB*0.5
481      VZZ(11,I2)=B5(2)+2.*B5(3)*SUB*0.5
482      IF (LP-2)      115,115,116
483      116 DO      117      I=3,LP
484      IQ1=I-1
485      IQ2=I+1
486      T=I
487      TE1=T*A5(IQ2)*(SUB*0.5)**IQ1
488      TE2=T*B5(IQ2)*(SUB*0.5)**IQ1
489      VRZ(11,I2)=VRZ(11,I2)+TE1
490      VZZ(11,I2)=VZZ(11,I2)+TE2
491      117 CONTINUE
492      115 CONTINUE
493      37 CONTINUE
494      PRINT      6030,  I1
495      6030 FORMAT (26H VRZ AT GRID POINTS ALONG 13,11HTH COLUMNS )
496      PRINT      223,  (VRZ(11,I2),I2=NSAVE,N2)
497      PRINT      6031
498      6031 FORMAT (20H      VZZ )
499      PRINT      223,  (VZZ(11,I2),I2=NSAVE,N2)
500      32 CONTINUE
501      PRINT      7072
502      7072 FORMAT      (60X,10HLOOP 32 OK      ///)
503      SUM2=0.
504      DO      40      I1=1,NSAVEB
505      IF (I1-2)      240,240,241
506      240 IF (I1-1)      242,242,243
507      242 N2=N2AA-N03
508      AREA=AREA1
509      DIST=DIST1
510      GO TO      244
511      243 N2=N2BB-N04
512      SUB=I1-1
513      DIST=0.5*SUB+DIST2
514      AREA=AREA2
515      GO TO      244
516      241 N2=NSAVEE
517      SUB=I1-1
518      DIST=0.5*SUB+DIST2
519      AREA=AREA2
520      244 CONTINUE
521      PRINT      130,  I1,NSAVEA
522      130 FORMAT(/40X,24HTHE STRESS COMPONENTS IN 13,9HTH COLUMN 7H:NSAVE=

```

```

1          13          )
523      PRINT 131
524      131 FORMAT (5X, 95HSR          SC          SZ
1          SRZ          J2          /)
525      SUM1=0.
526      IF (K1-1) 261,261,260
527      260 DO 41          I2=NSAVEA,N2
528      IF (I2-N2) 3001,3002,3002
529      3002 AREA=AREA/2.
530      3001 CONTINUE
531      ER=VRR(I1,I2)
532      EC=VR(I1,I2)/DIST
533      EZ=VZZ(I1,I2)
534      GAMA=VRZ(I1,I2)+VZR(I1,I2)
535      VA1=ER**2+EC**2+EZ**2
536      VA2=1.+(GAMA**2/(VA1+GAMA**2))
537      VA3=SQRT((0.5*VA1+0.25*GAMA**2)/(VA1**2))
538      VA5=(0.5*VA1+0.25*GAMA**2)/(VA1**2)
539      VA4=2.*3.14159*DIST*AREA*(VA2/VA5)*VA3
540      SUM1=SUM1+VA4
541      SR=1./SQRT(0.5*(1.+(EC**2/ER**2)+(EZ**2/ER**2))+0.25*(GAMA**2/ER**
12))
542      SC=1./SQRT(0.5*((ER**2/EC**2)+1.+(EZ**2/EC**2))+0.25*(GAMA**2/EC**
12))
543      SZ=1./SQRT(0.5*((ER**2/EZ**2)+(EC**2/EZ**2)+1.))+0.25*(GAMA**2/EZ**
12))
544      SRZ=1./SQRT(2.0*VA1/(GAMA**2)+1.00)
545      WJ2=0.5*(SR**2+SC**2+SZ**2)+SRZ**2
546      IF (NHD) 41,41,2002
547      2002 PRINT 132, SR,SC,SZ,SRZ,WJ2
548      132 FORMAT ( E12.5,5X, E12.5,10X,E12.5, 7X,E12.5,18X,E12.5 )
549      41 CONTINUE
550      GO TO 275
551      261 DO 42          I2=NSAVEA,N2
552      IF (I2-N2) 3003,3004,3004
553      3004 AREA=AREA/2.
554      3003 CONTINUE
555      ER=VRR(I1,I2)
556      EZ=VZZ(I1,I2)
557      GAMA=VRZ(I1,I2)+VZR(I1,I2)
558      VA1=ER**2+EZ**2
559      VA2=1.+(GAMA**2/(VA1+GAMA**2))
560      VA3=SQRT((0.5*VA1+0.25*GAMA**2)/(VA1**2))
561      VA5=(0.5*VA1+0.25*GAMA**2)/(VA1**2)
562      VA4=AREA*(VA2/VA5)*VA3
563      SUM1=SUM1+VA4
564      SR =1./SQRT(0.5*(1.+(EZ**2/ER**2))+0.25*(GAMA**2/ER**2))
565      SC =0.
566      SZ =1./SQRT(0.5*((ER**2/EZ**2)+1.))+0.25*(GAMA**2/EZ**2))
567      SRZ=1./SQRT(2.0*VA1/(GAMA**2)+1.00)
568      WJ2 =0.5*(SR **2+SZ **2)+SRZ **2
569      IF (NHD) 42,42,2003
570      2003 PRINT 273, SR,SC,SZ,SRZ,WJ2
571      273 FORMAT ( E12.5,5X, E12.5,10X,E12.5, 7X,E12.5,18X,E12.5 )

```

```
572      42 CONTINUE
573      275 PRINT  43, 11, SUM1
574      43 FORMAT ( / 30X, 10H THE SUM OF 13, 7HCOLUMN=E12.5      ///)
575      SUM2=SUM2+SUM1
576      40 CONTINUE
577      IF (NHD)      2004, 2004, 2005
578      2005 PRINT  45,      SUM2
579      45 FORMAT (32H THE TOTAL SUM OF THIS HALF MOLD=E12.5      )
580      2004 SUM=SUM+SUM2
581      1000 CONTINUE
582      ENE=RES*V
583      PRINT  46,      RES, SUM, ENE
584      46 FORMAT (20X, 30H THE MEASURED RESISTANCE FORCE=F10.2 /
1          20X, 30H THE COMPUTED ENERGY      =E12.5 /
1          20X, 26H COMPUTED R*V=      E12.5/      )
585      3000 CONTINUE
586      CALL EXIT
587      END
```

```

1      SUBROUTINE LEAST
2      COMMON X(21),Y(21),C(16),M,IP,LP,NR,NR1,CHECK
3      DIMENSION PIM1(50),PI(50),ALPHA(16),BETA(16),S(16),G(16),
4          1      PERR(50),T(3)
5          T(1)=2.8505852241
6          T(2)=-2.0751486497E-03
7          T(3)=-2.2520149609E-01
8          ZER=0.
9          ONE=1.
10         IF (LP-IP) 104,106,106
11         104 IP=IP
12         106 N=LP+1
13         K=IP+1
14         DO 130 I=1,M
15         PIM1(I)=ZER
16         PI(I)=ONE
17         130 CONTINUE
18         DO 140 I=1,16
19         S(I)=ZER
20         BETA(I)=ZER
21         ALPHA(I)=ZER
22         A1=ZER
23         B1=ZER
24         W11=M
25         I=1
26         160 WI=ZER
27         DO 170 L=1,M
28         WI=WI+Y(L)*PI(L)
29         S(I)=WI/W11
30         IF (I-N) 180,302,302
31         180 A1=ZER
32         DO 190 L=1,M
33         A1=A1+X(L)*PI(L)**2
34         A1=A1/W11
35         ALPHA(I+1)=A1
36         WI=ZER
37         DO 210 L=1,M
38         PIP1=(X(L)-A1)*PI(L)-B1*PIM1(L)
39         PIM1(L)=PI(L)
40         PI(L)=PIP1
41         WI=WI+PIP1*PIP1
42         210 CONTINUE
43         B1=WI/W11
44         BETA(I+2)=B1
45         W11=WI
46         I=I+1
47         GO TO 160
48         302 DO 310 L=2,16
49         310 G(L)=ZER
50         G(1)=ONE
51         DO 320 J=1,K
52         SJ=ZER
53         DO 320 L=1,K
54         G(L)=G(L)-ALPHA(L)*G(L-1)-BETA(L)*G(L-2)

```

```

54      S1=S1+S(L)*G(L)
55      320 CONTINUE
56      C(J)=S1
57      L=K
58      DO J40 I2=2,K
59      G(L)=G(L-1)
60      340 L=L-1
61      350 G(1)=ZER
62      IF (NR1) 404,405,404
63      404 PRINT 905, (J-1,C(J),J=1,K)
64      905 FORMAT (8E12.5)
65      405 CONTINUE
66      IF (CHECK) 1050,1050,1051
67      1051 PRINT 1035
68      1035 FORMAT (26HCoefficients ARE ***
69      LPP=LP+1
70      PRINT 1036, (C(I),I=1,LPP)
71      1036 FORMAT (10E12.5)

```